crystals

MDPI

Review

Borates—Crystal Structures of Prospective Nonlinear Optical Materials: High Anisotropy of the Thermal Expansion Caused by Anharmonic Atomic Vibrations

Rimma Bubnova [1,2,*], Sergey Volkov [1], Barbara Albert [3] and Stanislav Filatov [2]

[1] Institute of Silicate Chemistry, Russian Academy of Sciences, Makarov Emb. 2, St. Petersburg 199034, Russia; s.n.volkov@inbox.ru
[2] Department of Crystallography, Institute of Earth Sciences, St. Petersburg State University, University Emb. 7/9, St. Petersburg 199034, Russia; filatov.stanislav@gmail.com
[3] Eduard Zintl-Institute of Inorganic and Physical Chemistry, Technische Universität Darmstadt, Alarich-Weiss-Str. 12, 64287 Darmstadt, Germany; albert@ac.chemie.tu-darmstadt.de
* Correspondence: rimma_bubnova@mail.ru; Tel.: +7-981-181-3262

Academic Editors: Ning Ye and Rukang Li
Received: 7 February 2017; Accepted: 16 March 2017; Published: 22 March 2017

Abstract: In the present study the thermal structure evolution is reviewed for known nonlinear optical borates such as β-BaB_2O_4, LiB_3O_5, $CsLiB_6O_{10}$, $Li_2B_4O_7$, $K_2Al_2B_2O_7$, and α-BiB_3O_6, based on single-crystal and powder X-ray diffraction data collected over wide temperature ranges. Temperature-dependent measurements of further borates are presented for the first time: α-BaB_2O_4 (295–673 K), β-BaB_2O_4 (98–693 K), LiB_3O_5 (98–650 K) and $K_2Al_2B_2O_7$ (98–348 K). In addition to the established criteria for nonlinear optical (NLO) properties of crystals, here the role of the anisotropy and anharmonicity of the thermal vibrations of atoms is analysed as well as changes in their coordination spheres and the anisotropy of the thermal expansion of the crystal structure. Non-centrosymmetric borates, especially those that have NLO properties, often show distinct anisotropies for each cation in comparison to centrosymmetric borates. All considered NLO borates contain BO_3 triangles, which are the principal cause of the strong anisotropy of the thermal expansion.

Keywords: NLO borates; crystal structures at low and high temperatures; rigid boron–oxygen groups; anisotropic and anharmonic atomic vibrations; thermal expansion; low- and high-temperature single-crystal and powder X-ray diffraction

1. Introduction

In recent years, there has been extensive research and continuous development on second-order nonlinear optical (NLO) materials due to their potential applications. The revelation of the NLO effect on quartz crystals by Blombergen in 1962 [1] and the development of solid lasers in the early 1960s initiated huge progress in laser science and technology. In this context, the search for new NLO materials with optimized properties continues to be of special interest. Studies have shown that the second-order NLO properties of crystalline materials are closely related to their structures. Tens of inorganic and organic ([2–5], and Refs therein) crystals with NLO properties were identified, and their crystal structures, micro-structures, and various properties were studied. Nevertheless, there is growing interest in the search for new, prospective NLO materials due to the widening technical applications as a result of the replacement of gaseous and ionic laser sources with solid lasers. Basic principles of NLO material requirements, conditions of single crystal growing, studies of NLO properties, and applications are described in books, reviews, and multiple works [6–9].

There is a range of semi-empirical search criteria for NLO crystals. For example, the development of the Kurtz–Perry method [10] for instantaneous diagnostics of the second optical harmonic generation intensity considerably accelerated the screening for new NLO materials. Fast progress in the discovery of new NLO crystals was related with the works of Chen's team who developed the theory of anionic groups [11,12]. According to this theory, a certain type of anionic groups makes, as a first approximation, the main contribution to the second harmonic generation, although the contributions of the cations cannot be neglected either, according to the authors. The analysis of NLO properties, in particular of the NLO susceptibilities, and of structural data makes some prediction possible in the search for prospective crystals in one or another class of chemical compounds [13].

After the discovery of the NLO effect of $KB_5O_8{\cdot}4H_2O$ by Dewey and co-authors [14], the search for new NLO materials has focused on borates, due to the possibility of their application in UV and deep-UV regions. It turned out that NLO borates show many other properties that are necessary for a significant second harmonic generation. Borates have a wide spectral range of transparency combined with a high laser damage threshold, as well as good chemical and mechanical stability [3,12,15]. These properties make borates crucial materials for the generation of the second optical harmonic in UV and deep-UV regions. The theory of anionic groups made a considerable contribution to the revelation of new NLO borates [11,12]. Using this approach, NLO borates with different anionic groups were found: β-BaB_2O_4 [16], LiB_3O_5 [17], CsB_3O_5 [18], $Sr_2Be_2B_2O_7$ [19], $CsLiB_6O_{10}$ [20], and $K_2Al_2B_2O_7$ [21,22]. Later on, α-BiB_3O_6 [23], $BaBiBO_4$ [24] and many other NLO crystals were discovered [12]. For this reason, the structural behaviour of anionic groups consisting of boron and oxygen atoms is discussed in this review in detail.

Since the 1930s, when the first borate crystal structures were determined at ambient conditions by Zachariasen, Goldschmidt, Hauptmann and others, more than 2500 (re-)determined crystal structures of hydrous and anhydrous borates have been listed in the ICSD Database (ICSD-2016) up to now [25]. Modern descriptors of borate rigid groups, fundamental building blocks (FBBs) and finite clusters were introduced in [26–31]. The nomenclature of crystal structures and several classifications of borates have been described in a large number of review papers ([26–43] and Refs therein). As a result, the basic crystal chemistry principles of borates were established: (1) Boron atoms do occur equiprobably in both triangular and tetrahedral coordination to oxygen atoms and hydroxyl groups in the structures of crystals and glasses. (2) The BO_3 triangles or/and the BO_4 tetrahedra are connected via common corners (oxygen atoms) to form rigid cyclic 3B-groups composed from three of such polyhedra; several such groups can also be linked via shared BO_4 tetrahedra, thus forming multiple cyclic rigid groups. BO_4 tetrahedra scarcely share edges. These ways of condensation lead to the formation of boron–oxygen entities that do not change significantly in various crystals and glasses. (3) The rigid groups or their combinations linked by shared oxygen atoms constitute the fundamental building blocks (FBB) of the structure.

Due to the increased interest in borates, the thermal behaviour of these materials is currently being intensively investigated. The knowledge temperature-dependent changes of solids are required for the further development of crystal chemistry, solid state physics and chemistry, especially for the synthesis of materials and their applications. Our group has researched many years to identify new borates and study their crystal structures and thermal behaviour. In particular, we studied thermal expansion in a wide range of temperatures of more than 70 borates using powder X-ray diffraction [42–45], etc. and of dozens of borates using single-crystal X-ray diffraction [46–58]. Basic principles of the high-temperature crystal chemistry of borates were developed [26,42–44]. It was shown that BO_3 triangles, BO_4 tetrahedra and multiple cyclic 3B-groups remained practically invariable over a wide range of temperatures. We demonstrate that most of the borates show very strong anisotropies of the thermal expansion, even, in some cases, negative linear thermal expansion in certain directions [26,42–44], etc.

In this work the temperature-dependent structure evolution is reviewed for several NLO borates [47,49–57]. For anharmonic approximation [47,50,54] and behaviour under high pressure [59], several NLO borates are given as examples. Furthermore, new data from single crystal and

powder X-ray diffraction studies at low and high temperatures are presented for the first time: β-BaB_2O_4, LiB_3O_5 and $K_2Al_2B_2O_7$, measured within the intervals 98–693, 89–298 and 98–348 K, respectively. Finally, for the first time structural data on α-BaB_2O_4 at 295 and 673 K are discussed in an anisotropic approximation—unlike in the literature, where an isotropic approximation was chosen [60]. The main question is how the crystal structures of NLO borates change when the temperature increases. NLO borates studied in this work contain various rigid and non-rigid groups, and the dimensionality of the borate anions varies from 0D to 3D. Based on our observations, we derive trends for the high-temperature crystal chemistry of NLO borates.

Furthermore, we discuss the most eminent challenge within this research field—how to predict aprioristically the NLO properties of compounds. Accordingly, criteria are derived from crystal chemistry that allow for the identification of promising materials among a huge variety of compounds. We presume that the anisotropy and anharmonicity of thermal vibrations of atoms are very relevant, as well as the high anisotropy of the thermal expansion of crystals, amongst other reasons. Causes for the high anisotropy of NLO borates, as discussed in [44], are considered, too.

2. Thermal Evolution of the Structures of NLO Borates

Before discussing the main topic of this section, which is the structural variation of NLO borates that happens with temperature changes—we will give some general information about the crystal structures of borates under ambient conditions. This includes a brief description of the triangular BO_3 group and the tetrahedral BO_4 polyhedron in borates, the possibilities for polymerizing polyhedra and the formation of rigid and non-rigid B–O groups. Furthermore, we show their diversity, the notations and systematics, and we comment on how frequent polyanions of different dimensionality do occur.

2.1. Rigity and Flexibility of B–O Groups

B–O groups at ambient conditions. As mentioned in the introduction, borate anions are able to polymerize and form rigid groups. In the past, when more and more crystal structures were resolved, it became evident that rigid and almost uniform boron–oxygen groups are found in the structures of different crystalline and vitreous borates, as observed by Krogh-Moe [61,62]. Although the term "rigid boron–oxygen group" was introduced by Krogh-Moe half a century ago [61,62], the definition of the term has been given relatively recently [26,43]. *Rigid groups* are single polyhedra of BO_3 and BO_4 as well as cyclic triborate B–O rings composed of three polyhedra with common oxygen atoms at the corners and combinations of these 3B-rings. The latter may be connected *through shared tetrahedra* or common edges of the tetrahedra (at high-pressure synthesis [63–65]). Hence, these rigid groups can be considered as multiple (single, double, triple and so on) triborate (3B) groups, i.e., they are formed by condensation of single 3B-groups and share one or two common tetrahedra, independently of the multiplicity of the group. So, the simplest rigid group is a BO_3 triangle or a BO_4 tetrahedron like the TO_4 tetrahedron [66,67] in silicates, phosphates and others. Over the last few decades, high-density borates with unusual groups were synthesized by Huppertz and co-authors; their crystal structures show edge-sharing tetrahedra and were prepared by high pressure/high temperature synthesis [63–65].

If multiple rings are condensed via common oxygen atoms, they form flexible clusters. Such combinations are considered FBBs. "The FBB, by definition, should be the simplest unit that can reflect the basic structural information of an assigned crystallographic frame" [30]. The repeat unit of a borate can consist of one or several FBBs.

Notations of B–O groups. By the mid-1970s the main boron–oxygen groups containing one to six polyhedra were derived by Christ and Clark [68] and others. The history of the development of notations for B–O groups and FBBs was described in [26,28–31,43]. Boron–oxygen polyhedra start to polymerize when there is no lack of these polyhedra. Therefore, the anions of borates with a low content of B_2O_3 are mainly represented by isolated BO_3 triangles and BO_4 tetrahedra or non-cyclic diortho groups (dimers), e.g., two corner-sharing triangles in $[B_2O_5]$ and two corner-sharing

tetrahedra in $[B_2O_7]$. Isolated BO_3 and BO_4 polyhedra [30,35] are the most frequent anions. Starting from $n = 3$ (n is the number of boron atoms), the main groups appear to be cyclic.

Burns, Hawthorne and Grice [28,31] developed modern descriptors for the connectivity of borate polyhedra in every FBB after Christ and Clark [68], in particular in a ring. Borate polyhedra are written as Δ and □ depending on the coordination of the boron atom by three or four oxygen atoms, respectively. The elementary groups consisting of isolated $B\varphi_3$ triangles and isolated $B\varphi_4$ tetrahedra (φ = O, OH) are denoted as 1B:1Δ:Δ and 1B:1□:□ (1B:[(1:1T)], respectively (Figure 1, 1B:1Δ:Δ). The presence of more than one polyhedron in the descriptor indicates polymerization of the polyhedra by sharing corners; hence the group consisting of a triangle and a tetrahedron is written as 2B:1Δ1□:Δ□. The delimiters (< >) indicate that borate polyhedra form a single cyclic ring (Figure 1, 3B), and the signs '–' or '=' between two rings indicate that they share one or two tetrahedra, respectively (Figure 1, 4B, 5B). If an oxygen atom or any other anion (φ), polyhedron, or ring of polyhedra is bonded to more than two boron atoms, the φ is enclosed in the delimeters.

Symbols of the most frequently occurring triborate, tetraborate and pentaborate groups are 3B:3Δ:<3Δ>, 4B:2Δ2□:<Δ2□>=<Δ2□> and 5B:2Δ3□:<Δ2□>–<Δ2□>, respectively. According to the notation after Touboul, Penin, and Nowogrocki [29], these triborate, tetraborate and pentaborate groups are symbolized as 3:[3:(2Δ + T)], 4:[4:(2Δ + 2T)] and 5:[(3Δ + 2T)], respectively. On the basis of both of these approaches, modified descriptors for the description of rigid groups were worked out by Guan and Xue [30]. Modified descriptors after Burns, Grice and Hawthorne [28,31] are used in this review.

Non-cyclic groups (linear and branched complexes). The simplest non-cyclic groups are single polyhedra followed by groups of two and three polyhedra, called dimers and trimers. Their variety is caused by the substitution and rearrangement of tetrahedra and triangles (Figure 1, 1B). Single polyhedra and dimers are the most frequent.

Cyclic groups. Cyclic B–O groups are the result of polymerization and start to form at a considerable boron content above $M_xO_y:B_2O_3 = 1$ (modifying agent to boron oxide ratio). This means that they are forming from approximately the centre of the M_xO_y–B_2O_3 series for univalent and bivalent metals [34,43].

Double and multiple cyclic groups formed by condensation of triborate rings via shared polyhedra. Further condensation of single rings to form larger rigid B–O groups is realized via shared BO_4 tetrahedra. Several multiple groups are formed by condensation of single triborate groups consisting of three boron–oxygen polyhedra. In [28,31], all variants of polymers of boron–oxygen polyhedra (triangles and tetrahedra) that are possible were theoretically derived ($n < 6$, where n is the number of polyhedra in a group) (e.g., Figure 1).

Many of these groups were actually observed experimentally, some occurring often, some seldom. A unique example is the cyclic four-fold quad-tetraborate group 4B:{<3B>=<3B>}≡{<3B>=<3B>} (Figure 1, 4B:4□). It is formed by condensation of four triborate rings in a certain way: two groups are linked via two shared tetrahedra. This group of four BO_4 tetrahedra forming a large B_4O_{10} tetrahedron was first derived theoretically by Bokii and Kravchenko in 1966 [69]. All boron atoms in this 4B-group are tetrahedrally coordinated because each tetrahedron belongs to two 3B-rings. Recently, this large B_4O_{10} tetrahedron was experimentally found for the first time by Wu et al. in a borosilicate, $Cs_2B_4SiO_9$ (# 425583-ICSD), which has NLO properties in the deep-ultraviolet range [70]. In 2016, the 4B-group known as "supertetrahedron" was found in the new indium borate $In_{19}B_{34}O_{74}(OH)_{11}$, synthesized under high-pressure/high-temperature conditions by Huppertz et al. [71]. Furthermore, it is worth noting that $In_{19}B_{34}O_{74}(OH)_{11}$ is the first borate containing a supertetrahedron unit.

Non-rigid cyclic groups. Non-branched single rings consisting of a greater number of corner-sharing polyhedra ($n > 3$) seldom occur. When the number of corner-sharing polyhedra in a cyclic group is more than three, the group becomes non-rigid. A few structures are known that contain four polyhedra, mainly tetrahedra, for example finite 4B:4□:<4□> rings-clusters in $Ca_4Mg(CO_3)_2[B_4O_6(OH)_6]$ borcarite (80438-ICSD), infinite 4B:2Δ2□:∞^1<2Δ2□>—chains in $La(BO_2)_3$ (# 23609-ICSD), 4B:4□:∞^2<4□>—layers in $CaAlB_3O_7$ johadachidolite (# 10245-ICSD), and $CuTm_2(B_2O_5)_2$

(# 401327-ICSD). There exist six-membered rings of tetrahedra in the $MAl_2(B_4O_{10})O_{0.5}$ family, for example $NdAl_{2.07}(B_4O_{10})O_{0.6}$ (# 200666-ICSD) and $Bi_{0.96}Al_{2.37}(B_4O_{10})O$ (# 250428-ICSD), and eight-membered rings of alternative triangles and tetrahedra (Figure 1, 8B) in a layered polymorph of NLO α-BiB_3O_6 [72].

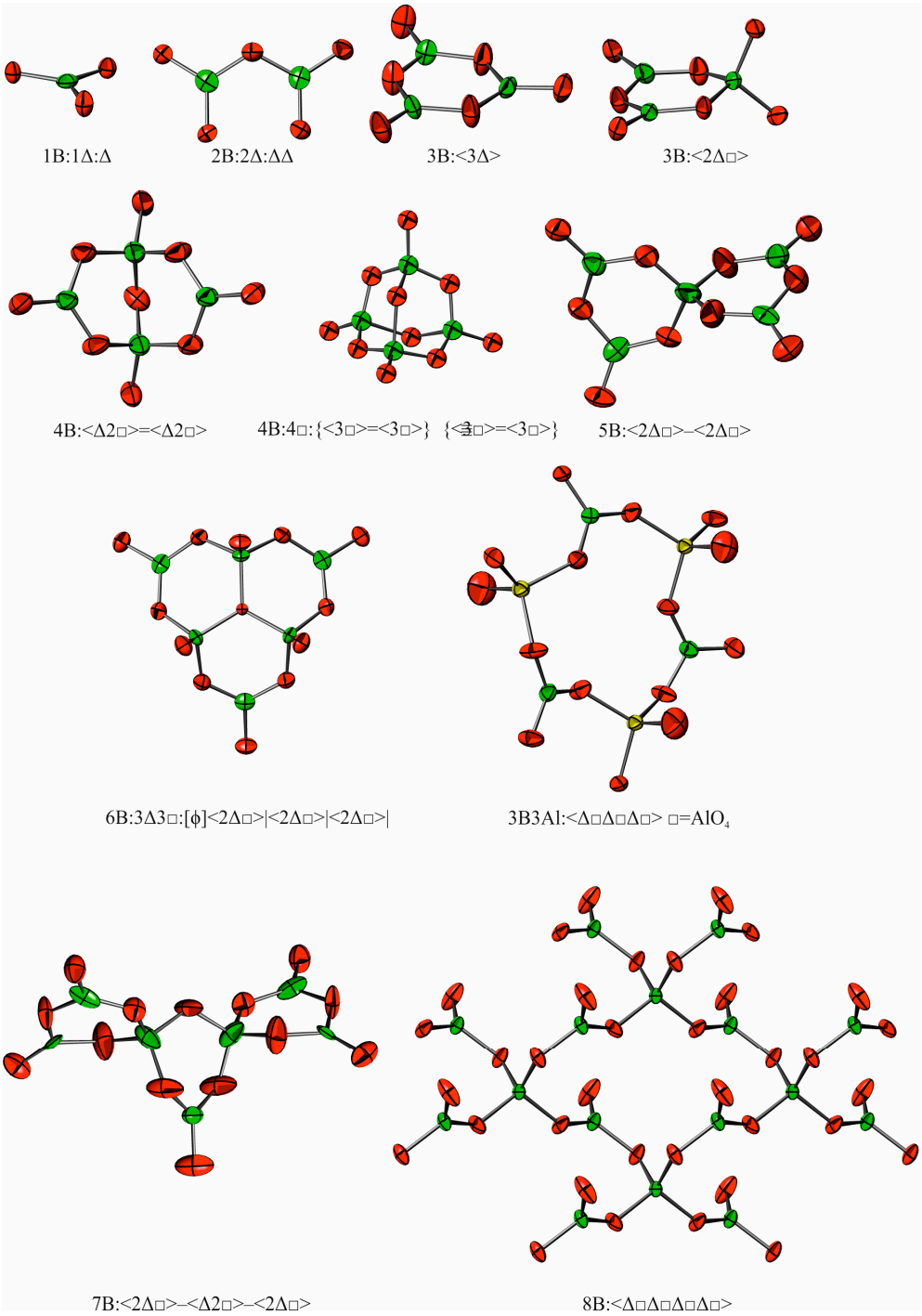

Figure 1. Main B–O groups occurring in NLO borates.

Occurrence of B–O polyanions of different dimensionality. Becker in 2001 as well as Guan and Xue in 2007 examined how often B–O polyanions of different dimensionality (the degree of polymerization—0D, 1D, 2D, 3D) do occur in 460 anhydrous [35] and 841 hydrous and anhydrous borates, respectively [30]. It was shown that the frequency of occurrence for borate anions in 460 anhydrous borates [35] is the following: isolated triangles and tetrahedra—52%, layers—15%, frameworks—12%, finite B–O groups—12%, infinite chains—9%. The distribution of boron–oxygen

groups in 841 borates [30] is as follows: isolated anions—55%, chains—12%, layers—11%, frameworks—22.6%. The frequency of occurrence of different FBBs was also represented in [30] with differentiation between non-centrosymmetric and centrosymmetric hydrated and anhydrous borates.

Thermal invariability of rigid B–O groups. Another common rule for borates (not only for those with NLO properties) is the invariability of rigid groups under conditions of variable temperatures. During the last two decades, the high-temperature crystal chemistry of borates has been developed intensively. Earlier, the thermal invariability of SiO_4 tetrahedra was shown and systematic variations of individual Si–O bond lengths in a tetrahedron as a function of the ligand oxygen atoms (bridging or nonbridging) were analysed at different temperatures [66,67], etc. There are not only BO_3 and BO_4 polyhedra, but also rigid B–O groups built up from these polyhedral, that are invariable on heating at first approximation, e.g., they maintain their configuration and size with changing temperature, as it was assumed earlier [34]. The suggestion was based on the high bond valence of considerably covalent B^{3+}–O bonds in BO_3 triangles (1 *v*. *u*. per each B–O bond in average) and BO_4 tetrahedra (3/4 *v*. *u*.). Our conclusion is also based on the invariability of rigid boron–oxygen groups in crystal structures of different borates.

The thermal invariability of rigid groups has been proven by single crystal HTXRD and LTXRD studies (HT, high temperature; LT low temperature) of about a dozen of borates [46–58], etc. These results have been summarized in [26,34,42,43] and are briefly described here. In this respect, the rigidity of a group means that the group cannot change its configuration as well as its size with varying temperature. It can be said that a rigid group is devoid of internal degrees of freedom. Therefore, borate structures constructed of rigid groups can react to temperature changes only by means of external degrees of freedom. An external degree of freedom of a rigid group is its ability to shift or to rotate as a unit relative to other groups around a mutual oxygen atom that serves as *a hinge*. Shear and hinge deformations are sharply anisotropic in nature [44].

Non-rigid cyclic groups. Corner-sharing BO_3 triangles and BO_4 tetrahedra can tilt and rotate around common oxygen atoms in a ring if the number of polyhedra exceeds three. These ways of sharing do not lead to rigid B–O groups and such "non-rigid" groups are not stable at high-temperature conditions. This can be illustrated by the examples of the 6B-ring in $K_2Al_2B_2O_7$ [21,22] and the 8B-ring in α-BiB_3O_6 [72], as described in the following paragraph.

2.2. Review of Temperature-Dependent Structural Studies of NLO Borates from Single-Crystal LTXRD and HTXRD Data

2.2.1. NLO Borates under Study

Here, we review the experimental results of single-crystal X-ray diffraction studies of NLO-borates in anisotropic and anharmonic approximation at low- and high-temperature conditions in the range of about 98 to 700 °C. To date, the thermal behaviour of the crystal structures of half a dozen NLO borates of different dimensionality from isolated BO_3 triangles and finite groups (0D) to double-framework (3D) were studied (Table 1). We also refined the structures of two NLO borates (LiB_3O_5 and $Li_2B_4O_7$) in anharmonic approximation, which had not been done for borates before [47,50]. Here these data are supplemented by new temperature-dependent structure data on the non-centrosymmetric β-BaB_2O_4 polymorph in comparison to centrosymmetric α-BaB_2O_4, recorded over a wide temperature range, and data for $K_2Al_2B_2O_7$ and LiB_3O_5 at low temperatures. Moreover, for the first time the crystal structure of α-BaB_2O_4 is refined in anisotropic approximation in addition to the isotropic one [60]. Structures of β-BaB_2O_4, $K_2Al_2B_2O_7$ and LiB_3O_5 are refined in anharmonic approximation, too. Temperature-dependent structure data and results of the thermal expansion tensor studied by the means of high-temperature powder X-ray diffraction are also discussed in parallel in Sections 3.4 and 3.5 (see Table 2 and comments).

For NLO borates like $K_2Al_2B_2O_7$, β-BaB_2O_4, LiB_3O_5, $CsLiB_6O_{10}$, and $Li_2B_4O_7$, thermal invariance of 1B-, 3B- and 4B-groups was observed, whilst for $K_2Al_2B_2O_7$ and α-BiB_3O_6 the thermal flexibility of non-rigid 6B- and 8B-groups was shown. Because NLO borates containing 5B-groups have not yet

been studied at elevated temperatures, we discuss the data for 5B-groups based on the structures of α-$Na_2B_8O_{13}$ [46] and α-CsB_5O_8 [48]. First, we consider systematic variations in B–O bond lengths with temperature and then the temperature-dependent structural behaviour of rigid groups and cations in NLO borates. We place an emphasis on the new data on NLO borates (Table 1 and Section 4).

Table 1. List of low- and high-temperature single-crystal XRD experiments for NLO borates.

Formula, Space Group, *Z*	FBB	Temperatures	References
Rigid groups			
$BaBiBO_4$, *Pnma*, *Z* 4	1B:1Δ:Δ		[58]
β-BaB_2O_4, *R*3*c*, *Z* 6	3B:3Δ:<3Δ>	98, 123, 173, 223, 295, 323, 693 K	this work
		163, 293 K	[49]
α-BaB_2O_4, *R*–3*c*, *Z* 6	3B:3Δ:<3Δ>	295, 673 K	this work
LiB_3O_5, *Pna*2$_1$, Z 4	3B:2Δ1□:∞^{3}<2Δ□>	98, 123, 148, 173, 198, 223, 248, 273, 298	this work
		293, 500, 650 K	[47]
$CsLiB_6O_{10}$, *I*–42*d*, Z 4	3B:2Δ1□:∞^{3}<2Δ□>	173, 193, 203, 213, 243, 293 K	[55]
$Li_2B_4O_7$, *I*4$_1$*cd*, Z 8	4B:2Δ2□:∞^{3}<Δ2□>=<Δ2□>	293, 473, 673, 773 K	[50]
		123, 148, 173, 198, 223, 248, 298 K	[51]
		10–290 K with steps of 10 K	[52]
		3.4–300 K	[53] *
		293–1203 K with steps of 20 K	[54] *
Non-rigid groups			
α-BiB_3O_6, *C*2$_1$, *Z* 2	8B:4Δ4□:∞^{2}<Δ□Δ□Δ□Δ□>	100, 140, 160, 180, 240, 295 K	[57]
$K_2Al_2B_2O_7$ **, *P*32$_1$, Z 3	6B:3Δ3□:∞^{3}<Δ□Δ□Δ□>	98, 123, 173, 223, 298, 348 K	this work

* Powder Rietveld refinement data; ** Aluminoborate $K_2Al_2B_2O_7$ consists of rings in which BO_3 triangles alternate AlO_4 tetrahedra.

2.2.2. Systematic Variations with Temperature of Boron–Oxygen Bond Lengths in NLO Borates

Variations of B–O bond lengths at ambient conditions. The distribution of boron–oxygen bond lengths and angles is of special interest due to capacity of boron atoms to be in triangular and tetrahedral coordination by oxygen. Average B–O bond lengths for triangles and tetrahedra are equal to 1.370 and 1.476 Å [31], respectively. Systematic variations in individual bond lengths were examined at ambient conditions by Filatov and Bubnova [26,34]. In contrast to SiO_4 tetrahedra [66,67] where the oxygen atoms can be bridging and non-bridging only, borate groups show additionally bridging oxygen atoms in different environments for boron atoms in triangular and tetrahedral coordination: (1) the $^{\Delta}O^{\square}$ oxygen atom links tetrahedral and triangular boron polyhedral; (2) the $^{\Delta}O^{\Delta}$ atom links a triangle with a triangle; (3) the $^{\square}O^{\square}$ atom links a tetrahedron with a tetrahedron; (4) and finally non-bridging (O^{Δ} and $O^{\square}$) oxygen atoms can exist in both polyhedra. Thus, there exist systematic differences between the individual bond lengths within a group according to the second Pauling's rule: (a) for the bridging B–O bonds (<$B^{\square}$–$^{\square}O^{\Delta}$> > <$B^{\square}$–$^{\square}O^{\square}$> > <B^{Δ}–$^{\Delta}O^{\Delta}$> > <B^{Δ}–$^{\Delta}O^{\square}$>) and (b) for terminating B–O bonds (<B^{Δ}–$^{\Delta}O^{\Delta}$> > <B^{Δ}–O^{Δ}> and <$B^{\square}$–$^{\square}O^{\Delta}$> > <$B^{\square}$–$O^{\square}$>). When the temperature increases, these trends remain [26].

Thermal variations of B–O bond lengths. Like silicates [73], the borates under study (see Section 4) show a weak contraction of the majority of individual and average strong and short B–O bond lengths when temperature changes, as it was observed in previously studied α-$Na_2B_8O_{13}$ [46], LiB_3O_5 (20–400) [47], α-CsB_5O_8 [48], and $Li_2B_4O_7$ [50,51]. The results of these studies were summarized in [26].

This contraction is an artefact of the X-ray diffraction method. It is caused by atomic thermal vibrations. When the bonds are strong in a group of atoms like TO_3 and TO_4 polyhedra, the entire group may undergo oscillation. This was called rigid body motion by Cruickshank [74]. The motion of each atom of the group is caused by the motion of the group. The effect of the thermal motion on bond lengths changes was first estimated from diffraction measurements by Busing and Levy [75]. Rigid body criteria were summarized by Downs ([73,76,77], and Refs therein). The atomic coordinates resulting from a single-crystal X-ray diffraction experiment are the maxima or the

centroids of the electron density arising from the combined effects of atomic positions and thermal displacements. When temperature increases, the bond lengths change due to thermal atomic vibrations. The contraction can be described by the model of rigid-body motion [73–77]. Bond lengths are corrected according to the model of rigid-body motion using the formula given in [73,76]:

$$R_{corr}^2 = R_{obs}^2 + \frac{3}{8\pi^2}(B_{eq}(A) - B_{eq}(C)), \quad (1)$$

where R_{corr} and R_{obs} are corrected and observed B–O bond lengths, correspondingly; $B_{eq}(A)$ and $B_{eq}(C)$ are equivalent displacement parameters of the anion (oxygen) and the cation (boron, aluminium), correspondingly.

After applying this correction, the mean B–O bond lengths tend to increase slightly upon heating. This approach was described for borates in [26], and is applied here for the NLO borates under study (Figure 2). Individual B–O bond lengths are given as a function of temperature for β-BaB_2O_4 (a) and LiB_3O_5 (c). For $K_2Al_2B_2O_7$, Al–O bond lengths are shown in Figure 2b. In a temperature range of 23 to 1000 °C a mean thermal expansion for Al–O bond lengths in AlO_4 tetrahedra of zero was described by Hazen, Prewitt and Finger [66,67]. In the present study negative thermal expansion is found for the Al1–O1 and Al2–O2 bond lengths of AlO_4 tetrahedra in the range of 100–400 K (Figure 2b).

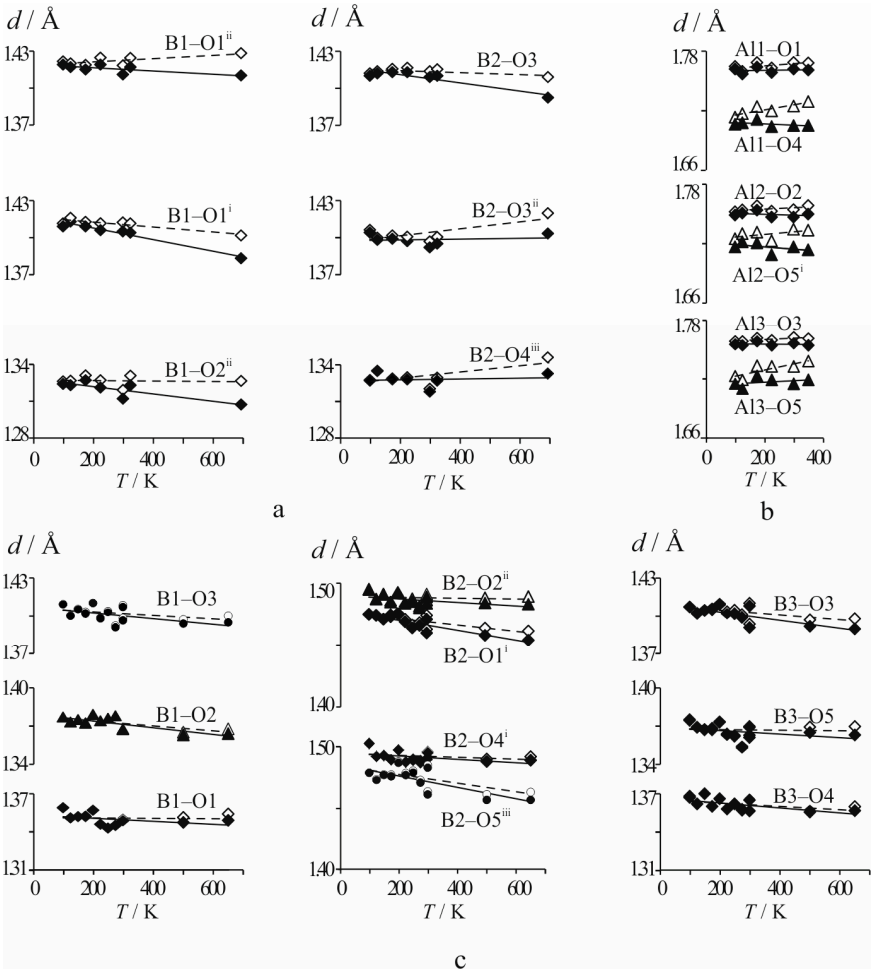

Figure 2. Temperature dependence of B–O bond lengths in the structures of β-BaB_2O_4 (**a**), of Al–O bond lengths in $K_2Al_2B_2O_7$ (**b**) and of B–O bond lengths in LiB_3O_5 (**c**). Observed values are shown in dark signs and solid lines; values after introduction of a correction according to Downs [75,76] are shown in light signs and dashed lines. Symmetry codes for β-BaB_2O_4: (i) $-x + y, -x, z$; (ii) $x, x - y, z - 1/2$; (iii) $-y, x - y, z$. Symmetry code for $K_2Al_2B_2O_7$: (i) $y, x, -z$. Symmetry codes for LiB_3O_5: (i) $x, y - 1, z$; (ii) $-x + 1, -y + 1, z + 1/2$; (iii) $-x + 3/2, y - 1/2, z - 1/2$; (iii) $-x + 3/2, y + 1/2, z + 1/2$.

2.2.3. Thermal Invariability of Rigid B–O Groups in NLO Borates

The structures of the vast majority of existing NLO borates are based upon isolated BO_3 triangles. Those with single cyclic 3B-, double cyclic 4B- and 5B-groups of different dimensionality occur frequently in NLO borates; other groups occur occasionally. The main groups that occur in NLO borates are represented in Figure 1. Hence, at first we will consider thermal vibrations of the single BO_3 triangles. As an example, we discuss the $Ca_4REEO(BO_3)_3$ family [12] which is related to NLO borates based on isolated BO_3 triangles where *REE* = Gd (# 39716-ICSD) or Y, as well as $K_2Al_2B_2O_7$ [21] and $BaBiBO_4$ [24]. We have investigated $K_2Al_2B_2O_7$ (see Section 4.3) and $BaBiBO_4$ [58]. Nevertheless, the description of these borates is not uniquely defined: $K_2Al_2B_2O_7$ can be considered also as boroaluminate framework composed of non-rigid six-membered rings in which BO_3 triangles alternate with AlO_4 tetrahedra (see Section 4.3), and $BaBiBO_4$ can also be described as being built up from rigid borate-bismuthate chains. There are inconsistent data on the symmetry and NLO properties of $BaBiBO_4$: it was firstly determined as crystallizing in the non-centrosymmetric space group $Pna2_1$ with NLO properties (# 154105-ICSD, [24]), whilst later it was refined in space group *Pnma* (# 9424596-ICSD, [58]). In any case, in both borates, $K_2Al_2B_2O_7$ (see Section 4.3) and $BaBiBO_4$ [58], the BO_3 triangles exhibit thermal invariability (see Figure S1c).

There are four triborate rings that can be derived by permuting triangles for tetrahedra: (1) a ring of three triangles, 3B:<3Δ>; (2) a ring of two triangles and a tetrahedron, 3B:<2Δ□>, (3) a ring of a triangle and two tetrahedra, 3B:<Δ2□>; and (4) a ring of three tetrahedra, 3B:<3□>. Two of them, <3Δ> and especially <2Δ□> (see Figure 1, 3B) occur frequently in NLO borates. All triborates of univalent metals except for the two modifications of α- and β-NaB_3O_5 are also built up from <2Δ□> 3B-groups. These are the topologically identical three-dimensional frameworks of LiB_3O_5 (# 1585-, 66708-ICSD), CsB_3O_5 (# 2081-ICSD), $CsLiB_6O_{10}$ (# 80826-ICSD), TlB_3O_5 (#84855-ICSD), α- and β-RbB_3O_5 (# 91545, 87519-ICSD)-, and also another framework of KB_3O_5 (250224-ICSD). Most of them are borates with excellent NLO properties.

Among 4B-groups the 4B:<Δ2□>=<Δ2□> double ring (see Figure 1, 4B) is common in NLO borates ($Li_2B_4O_7$ (23876-, 34670-, 300010-, 65930-ICSD), $LiNaB_4O_7$ (186901-ICSD) etc. A unique four-fold cyclic 4B-group is formed by a condensation of four 3B-rings 4B:{<3B>=<3B>}≡{<3B>=<3B>} (see Figure 1, 4B:4□). It occurs only in the borosilicate $Cs_2B_4SiO_9$ (# 425583-ICSD) which shows NLO properties in the deep-ultraviolet range [70].

Double 5B-groups <3B>–<3B> composed of two 3B-rings via a common tetrahedron (see Figure 1, 5B) occur quite frequently for instance 5B:4Δ1□:<2Δ□>–<2Δ□> in $K[B_5O_6(OH)_4]\cdot 2H_2O$ (18211-ICSD), 5B:3Δ2□:<2Δ□>–<2Δ□> in $K_2SrVB_5O_{12}$ (185934-ICSD), 5B:2Δ3□:<2Δ□>–<2Δ□> in $La_2CaB_{10}O_{19}$ (92866-ICSD).

The following groups occasionally occur in NLO borates: 2B:2Δ:ΔΔ in $Pb_4O(BO_3)_2$ (261420-ICSD), 6B:3Δ3□:[O]<Δ2□>|<Δ2□>|<Δ2□>| in $K_3B_6O_{10}Cl$ (262005-ICSD), 7B:5Δ2□:<2Δ□>–<Δ2□>–<2Δ□> in $Li_4Cs_3B_7O_{14}$ (261420-ICSD) (see Figure 1, 7B). FBBs composed of two rigid groups are rare but do occur, for instance in $LiKB_4O_7$ (93601-ICSD) and $LiRbB_4O_7$ (93602-ICSD).

Thermal variations of B–O–B angles. As defined in Section 2.1 a rigid group is devoid of internal degrees of freedom whilst the external degrees of freedom of a rigid group change as impact on temperature. In other words, angles between polyhedra have to be almost invariable within the group and changeable between groups with temperature varying. This will now be discussed for different rigid groups:

In isolated *triborate* <3Δ>*3B-groups* (β-BaB_2O_4) the average change in the B–O–B angles equals 0.6° in the range of 98 to 693 K (Section 4.1).

Tetraborate groups ($Li_2B_4O_7$ [50,51]) have B–O–B angles in the triangles and tetrahedra forming the rigid group that change by 0.1° whilst the angles between the rigid groups change by 1.6° on average.

The *pentaborate group* (α-CsB_5O_8 [48] and α-$Na_2B_8O_{13}$ [46]) contains six independent B–O–B angles within the group. Among them, the mean changes of the values of the angles do not exceed 0.5°. However B–O–B angles between the groups increase by 1.9°–2.3°.

Summary. The conclusion can be drawn that—at least in the temperature range of 20 to 500 °C—the variations of B–O–B angles within rigid groups are usually equal or less than 0.5°. This

value is comparable with the error bars. For the same temperatures, the angles between rigid groups vary over a wider range (about 2°). The B–O bond lengths are almost invariable within accuracy of experiment (Section 2.2.2). Thus the thermal evolution of rigid groups in NLO borates shows that they are thermally invariable ([26,34]; see Sections 4.1–4.3).

2.2.4. Non-Rigid Cyclic Groups in NLO Borates

As discussed in Section 4.3 when analysing $K_2Al_2B_2O_7$, AlO_4 tetrahedra are located in a flexible six-fold ring that is composed of alternating BO_3 triangles and AlO_4 tetrahedra (see Figure S1d). The *T*–O bond lengths (in this case *T* = Al) practically do not change with temperature both in rigid and non-rigid groups because the TO_4 tetrahedron is a trivial rigid group. As for O–O–O angles, they change both inside the six-fold ring and outside of it (see Section 3.6), and the changes can reach 2°.

Another flexible ring consisting from eight alternating BO_3 triangles and BO_4 tetrahedra is present in the layered polyanion of the NLO borate α-BiB_3O_6 [72] (see Figure 1, 8B). Here, the angles change by more than 0.5° in a relatively small temperature range of 200 K (100–295 K) (see Section 3.6), and it reaches a more considerable value of 1.5° after increasing the range to 400°.

Interatomic O–O distances in BO_3 triangles and BO_4 tetrahedra of the eight-fold ring practically do not change with temperature. A value of zero given for the O–O edge of the polyhedron means that in the mentioned range of temperatures the changes do not exceed the measurement error of 0.5°.

Summary. One can conclude that, unlike in the rigid groups, the angles within the non-rigid B–O groups change with temperature. This holds for angles between polyhedra both inside the ring and outside. Changes of the interatomic O–O distances in the polyhedra are within the limits of 0.02 and 0.04 Å for both rigid and non-rigid groups.

2.3. Anisotropic Thermal Expansion of Borates from Powder HTXRD Data

In parallel to temperature-dependent structural studies the thermal expansion of more than 70 borates including many NLO borates has been examined by high-temperature X-ray powder diffraction (in air). The results have been published before in [26,34,42,43], etc. and are summarized in Table 2. They are also supplemented by more recent data obtained after 2013, also given in Table 2. Here, except for the formula of the compound, its symmetry, the studied temperature range (Δt) and the reference of the source, the tensor of the thermal expansion coefficients α_{11}, α_{22}, α_{33} is given, the expansion coefficient α_V of the volume and the difference $\Delta = \alpha_{max} - \alpha_{min}$. The borates are assigned to groups according to the cation. There are more than two dozen non-centrosymmetric borates that are marked in bold in Table 2, and nearly half of them generate a second harmonic (marked by asterisks). A more detailed data analysis of Table 2 is given later on (Section 3).

Table 2. Main characteristics of the thermal expansion of borates.

Compound	System, Space Group	$\alpha \times 10^6$ K^{-1}					Δt, °C	Refs
		α_{11}	α_{22}	α_{33}	α_V	$\alpha_{max} - \alpha_{min}$		
Li–borates								
$Li_2B_4O_7$ *	**Tetrag., *I*4$_1$*cd***	**17**	**17**	**−13**	**21**	**30**	−189–27	[51]
		16	**16**	**−4**	**28**	**20**	20–250	[50]
		16	**16**	**12**	**44**	**4**	250–750	
$LiCsB_6O_{10}$ *	**Tetrag., *I*–42*d***	**20**	**20**	**−22**	**18**	**42**	25–600	[55]
$Li_3B_{11}O_{18}$	Monocl., *P*2$_1$/*a*	14	38	−16	36	54	20–180	[78]
LiB_3O_5 *	**Orth., *Pna*2$_1$**	**101**	**31**	**−71**	**61**	**172**	25–530	[47]
		66	**29**	**−63**	**32**	**129**	25–790	[79]
		108	**34**	**−88**	**54**	**196**	25–790	[80]

Na–borates								
$Na_2B_4O_5(OH)_4{\cdot}3H_2O$	**Trigon., *R*32**	**14**	**14**	**11**	**39**	**3**	0–80	[81]
γ–$Na_2B_4O_7$	Tricl., *P*–1	16	12	4	32	12	20–550	[56]
$BaNaSc(BO_3)_2$	Trigon., *R*–3	8	8	21	38	13	20–550	[82]
α–$Na_2B_4O_7$	Tricl., *P*–1	25	20	9	54	16	20–700	[83]
$BaNaY(BO_3)_2$	Trigon., *R*–3	6	6	26	38	20	25	[82]
		19	19	11	49	8	300	
$Na_3(NO_3)B_6O_{10}$	Orth., *Pnma*	8	9	39	56	31	20–700	[26]
α-$Na_2B_8O_{13}$	Monocl., *P*2$_1$/*a*	34	11	1	46	33	300	[46]
β-$Na_2B_8O_{13}$	Monocl., *P*2$_1$/*c*	15	38	−1	52	39	20–600	[26]
β-NaB_3O_5	Monocl., *P*2$_1$/*c*	33	−7	6	32	40	20–700	[83]
$Na_2B_4O_6(OH)_2{\cdot}3H_2O$	Monocl., *P*2$_1$/*c*	43	24	0	67	43	0–80	[81]
$(K_{0.5}Na_{0.5})_3B_9O_{15}$	Monocl., *P*2$_1$/*c*	49	5	7	61	44	20–700	[84]
$Na_2B_4O_5(OH)_4{\cdot}8H_2O$	Monocl., *C*2/*c*	77	−2	19	80	79	4–30	[81]
K–borates								
$K_2Al_2B_2O_7$ *	**Trigon., *P*32**	**8**	**8**	**17**	**33**	**9**	30–295	[85]
$K_5B_{19}O_{31}$	Monocl., *C*2/*c*	18	3	3	24	15	20–700	[34]
α-KB_5O_8	Orth., *Pbca*	12	12	−4	20	16	20–370	[86]
		12	12	5	29	7	370–550	
KB_3O_5	Monocl., *P*2$_1$/*c*	37	3	6	46	34	20–650	[87]
$K[B_5O_6(OH)_4]{\cdot}2H_2O$ *	**Orth., *Aba*2**	**7**	**18**	**44**	**69**	**37**	20–115	[88]
$K_2NaB_9O_{15}$	Monocl., *P*2$_1$/*c*	52	3	0	55	52	20–650	[84]
β-KB_5O_8	Orth., *Pbca*	60	20	−3	77	63	200–700	[34]
Rb–borates								
$Rb_2B_4O_7$	Tricl., *P*–1	20	25	12	57	13	20–700	[89]
$Rb_5B_{19}O_{31}$	Monocl., *C*2/*c*	27	3	11	41	24	20–600	[90]
α-RbB_5O_8	Orth., *Pbca*	5	10	−14	1	24	150–300	[86]
		5	10	30	45	25	300–500	
$Rb_3B_7O_{12}$	Tricl., *P*–1	54	9	2	65	52	20–600	[91]
β-RbB_5O_8	Orth., *Pbca*	61	23	5	89	56	20–720	[92]
$RbB_5O_6(OH)_4{\cdot}2H_2O$ *	**Orth., *Aba*2**	**77**	**−20**	**21**	**78**	**97**	20–100	[88]
α-RbB_3O_5	**Orth., *P*2$_1$2$_1$2$_1$**	**29**	**−27**	**74**	**76**	**101**	20–600	[93]
β-RbB_3O_5	**Orth., *P*2$_1$2$_1$2$_1$**	**18**	**−11**	**89**	**96**	**100**	20–700	[93]
$Rb_{0.9}Cs_{0.1}B_3O_5$	**Orth., *P*2$_1$2$_1$2$_1$**	**24**	**−40**	**73**	**57**	**113**	20–700	[94]
Cs–borates								
CsB_3O_5 *	**Orth., *P*2$_1$2$_1$2$_1$**	**23**	**11**	**48**	**82**	**37**	20–800	[34]
β-CsB_5O_8	Orth., *Pbca*	53	16	14	83	39	20–540	[95]
α-CsB_5O_8	Monocl. *P*2$_1$/*c*	27	61	−8	80	69	20–600	[48]
$CsB_5O_6(OH)_4{\cdot}2H_2O$	Monocl. *A*2/*a*	83	18	4	100	79	20–95	[88]
NH_4–borates								
$(NH_4)_3[B_{15}O_{20}(OH)_8]{\cdot}4H_2O$	Monocl. *C*2/*c*	28	41	18	87	23	10–80	[96]
$NH_4B_5O_8$	Orth., *Pbca*	39	6	20	65	33	20–330	[97]
$NH_4[B_5O_7(OH)_2]{\cdot}H_2O$	Monocl. *P*2$_1$/*c*	32	53	−3	82	56	20–90	[98]
Ca–borates								
$CaMg[B_3O_4(OH)_3]_2{\cdot}3H_2O$	Monocl. *P*2/*c*	16	18	10	44	8	20–270	[99]
$Ca[B_3O_4(OH)_3]{\cdot}H_2O$	Monocl. *P*2/*a*	29	29	−11	47	40	20–300	[100]
Sr–borates								
SrB_4O_7	**Orth., *Pmn*2$_1$**	**7**	**9**	**8**	**24**	**2**	20–900	[101]
$Sr_2B_{16}O_{26}$	Monocl. *P*2/*c*	21	10	4	35	17	20–740	[101]
γ-$Sr_2B_2O_5$	Monocl. *P*2/*c*	20	7	1	28	19	20–292	[102]
SrB_2O_4	Orth., *Pbcn*	4	4	33	41	29	20–900	[101]
$Sr_3B_2O_6$	Trigon., *R*–3*c*	10.5	10.5	44	65	33.5	20–900	[101]
Ba–borates								
$LiBaB_9O_{15}$	Trigon., *R*–3*c*	7	7	−5	9	12	20–700	[103]
α-BaB_2O_4	Hex., *R*–3*c*	6	6	28	40	22	20–700	Here
BaB_4O_7	Monocl., *P*2$_1$/*c*	23	−12	5	16	35	20–700	[104]
β-BaB_2O_4 *	**Trigon., *R*3*c***	**3**	**3**	**45**	**51**	**42**	20–700	[104]

Bi–borates								
$Bi_{24}B_2O_{39}$	**Cub., *I*23**	**17**	**17**	**17**	**51**	**0**	20–600	[43]
$Ba_3Bi_2(BO_3)_4$	Orth., *Pnma*	16	11	11	38	5	25	[105]
		30	12	10	52	20	500	
$Ba_2Bi_3B_{25}O_{44}$	Trigon., *R*–3*m*	12	12	6	30	6	25	[106]
		12	12	0	24	12	700	
$Bi_3B_5O_{12}$	Orth., *Pnma*	12	12	3	27	9	20–700	[107]
$SrBi_2B_4O_{10}$	Tricl., *P*–1	13	9	2	24	11	20–700	[108]
$Bi_4B_2O_9$	Monocl., $P2_1/c$	20	15	6	41	14	20–500	[109]
$BaBiBO_4$	Orth., *Pnma*	28	6	10	22	44	25	[58]
		42	−3	12	51	45	700	
$BaBi_2B_2O_7$	**Hex., $P6_3$**	**6**	**6**	**20**	**32**	**14**	25	[110]
		8	**8**	**34**	**50**	**26**	625	
$BaBi_2B_4O_{10}$	Monocl., $P2_1/c$	13	11	−3	21	16	20	[111]
		13	11	4	28	9	150	
		31	11	9	51	22	600	
$Sr_{0.5}Ba_{0.5}Bi_2B_2O_7$	**Hex., $P6_3$**	**3**	**3**	**22**	**29**	**19**	25	[110]
		9	**9**	**33**	**50**	**24**	625	
$SrBi_2B_2O_7$	**Hex., $P6_3$**	**4**	**4**	**22**	**30**	**18**	25	[110]
		8	**8**	**30**	**46**	**22**	625	
***α*-$Bi_2B_8O_{15}$**	**Monocl., *P*2_1**	**2**	**49**	**−8**	**43**	**57**	20–300	[112]
		8	**30**	**2**	**40**	**28**	300–700	
***α*-BiB_3O_6 ***	**Monocl., *C*2**	**−28**	**54**	**8**	**34**	**82**	−200–300	[113]
		−25	**54**	**10**	**39**	**79**	−253–525	[57]
***REE*–borates**								
π-$NdBO_3$	Hex., *P*63/*mmc*	15	15	13	43	2	20	[114]
		14	14	2	30	12	540	
λ-$NdBO_3$	Orth. *Pnma*	22	15	17	54	7	20	[115]
		21	3	7	37	18	820	
π-$LuBO_3$	Monocl., *C*2/*c*	9	9	2	20	7	20	[114]
		8	8	1	17	7	540	
β-$LuBO_3$	Trigon., *R*–3*c*	2	2	13	17	11	20–600	[114]
Mixed borates								
$LuBa_3B_9O_{18}$	Hex., $P6_3/m$	3	3	39	39	36	20–900	[116]
Fe_3BO_6	Orth. *Pnma*	14	12	2	28	12	20	[117]
		11	9	10	29	2	800	
$KZnB_3O_6$	Tricl., *P*–1	−1	1	45	45	46	100–740	[118]
$Zn_4B_6O_{13}$	**Cub., *I*–43*m***	**0.3**	**0.3**	**0.3**	**1**	**0**	−260–−163	[119]
		1	**1**	**1**	**3**	**0**	−163–−3	
$LiBeBO_3$	Tricl., *P*–1	**−3.3**	**1.8**	**7.6**	**6.1**	**10.9**	−200–−80	[120]
$GdCa_4O(BO_3)_3$ *	**Monocl., *Cm***	**12 ****	**5 ****	**6 ****	**23 ****		23–300	[12]
$YCa_4O(BO_3)_3$ *	**Monocl., *Cm***	**13**	**4**	**25**	**43**	**21**	27	[121]
		13	**5**	**30**	**48**	**25**	100	
$La_2CaB_{10}O_{19}$ *	**Monocl., *C*2**	**9 ****	**8**	**2 ****	**19 ****		25–300	[122]
$Na_3La_9O_3(BO_3)_8$ *	**Hex., *P*–62*m***	**8**	**8**	**15**	**31**	**7**	30–500	[123]

Non-centrosymmetric borates are marked by bold. * NLO borates; ** Thermal expansion coefficients are given along the *a*-, *b*-, and *c*-axes (eigenvalues of thermal expansion tensor were not calculated for monoclinic crystals).

3. Discussion. Desirable Crystal Chemical Criteria for NLO Borates

Here we consider desirable crystal chemical criteria for NLO crystals based on experimental data revealed in the present study. Besides the manifestation of the anisotropy of the optical properties (strong birefringence), we propose to analyse a few more possible conditions.

As discussed by us for the first time [47], "nonlinear optical effects might be caused by the anharmonicity of atomic thermal displacements that can be seen in thermal expansion tensor and in deviations from Gaussian shape of the probability density function of atomic thermal displacement

factors". Particularly, the thermal expansion tensor coefficients analysis (see Table 2) of two dozens of non-centrosymmetric borates versus centrosymmetric ones showed that most of the NLO borates expand strongly anisotropic.

3.1. Anharmonicity of Atomic Vibrations in NLO Materials

Up to date, there are only a few structures of nonlinear borates refined in the anharmonic approximation, i.e., LiB_3O_5 [47], $Li_2B_4O_7$ [50,54] and β-BaB_2O_4 (Table S4). It has been found that the atomic vibrations of Li atoms are asymmetrical more strongly than those of Ba atoms (Figure 3). At the same time, the anharmonic parameters for B and O atoms are of the same order as their estimated standard deviations (ESDs). Anharmonic parameters for Ba atoms exceed their error bars whilst B and O atoms vibrate practically anisotropically. The strongest anharmonicity of vibrations of Li atoms is found in LiB_3O_5.The thermal vibrations figure of the Li atom is oliform (Figure 3a), narrower on one side and wider on the other. The anharmonic vibrations of the Li atom are weaker in $Li_2B_4O_7$ (Figure 3b), and the vibrations of the Ba atoms in β-BaB_2O_4 are the weakest (Figure 3c). It is remarkable that the NLO properties are also expressed weaker in $Li_2B_4O_7$ than in LiB_3O_5 [12,15], etc. This can be caused by the stronger anharmonicity of the Li atoms' vibrations. The anharmonicity increases sharply with temperature in LiB_3O_5 [47] and in $Li_2B_4O_7$ [50,54], especially close to the melting point, as found by Senyshyn and co-authors [54].

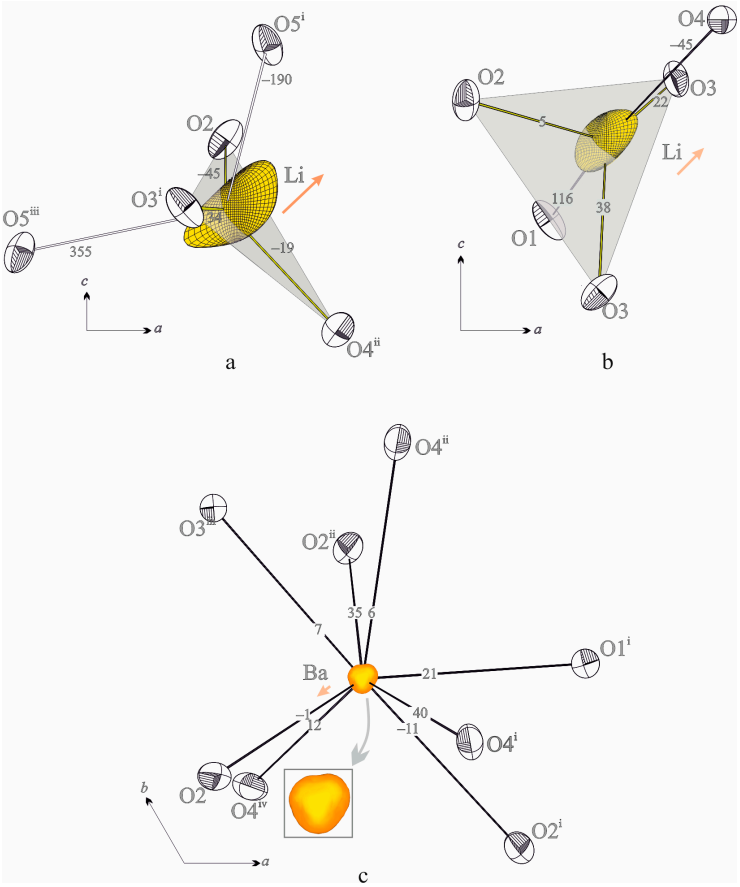

Figure 3. Comparison of the figures of thermal vibrations in an anharmonic approximation for LiB_3O_5 at 650 K after [47] (**a**); $Li_2B_4O_7$ at 773 K after [50] (**b**) and β-BaB_2O_4 (**c**) [present work] at 298 K. Oxygen atoms are given in harmonic approximation with probability of 88%. The twofold increased fragment image of Ba figure of anharmonic thermal vibrations is shown. Near Ba–O and Li–O bonds, their coefficients of thermal expansion (× 10^6 K^{-1}) are shown. The arrows next to the lithium and barium atoms show the direction of their displacement with temperature. Symmetry codes for LiB_3O_5: (i) $-x + 1, -y + 1, z - 1/2$; (ii) $x - 1/2, -y + 3/2, z - 1$; (iii) $x, y, z - 1$. Symmetry codes for β-BaB_2O_4: (i) $-y + 2/3, -x + 1/3, z - 1/6$; (ii) $-x + y + 1/3, -x + 2/3, z - 1/3$; (iii) $-y + 1/3, -x + 2/3, z + 7/6$; (iv) $-x + y, y, z - 1/2$.

In general, the character of thermal vibrations of the atom is largely determined by its environment. Anharmonic vibrations may indicate a sharp asymmetry of the atom environment. According to [51,54], the Li atom, being in the channel of the double boron–oxygen framework of $Li_2B_4O_7$ borate, preferably oscillates along this channel. It gives another possible structural criterion of NLO materials—irregular coordination of the atoms.

3.2. High Mobility of Cations in NLO Borates

Thermal decreasing of cation coordination. The Li coordination at room temperature is described in [124] as a distorted tetrahedron where the Li atom is displaced from the centre towards the O2O3O4 plane (Figures 3a and 4a). Thus, Li atoms are coordinated by four oxygen atoms with the Li–O bond lengths being 1.979–2.180 Å [47]; the next oxygen $O5^{iii}$ atom is at a distance of 2.684 Å from Li. The distorted LiO_4 tetrahedron (Figure 3a) at low (see Section 4.2) and room temperature transforms into a triangle at 377 °C [47]. Three bond lengths (Li–O2, Li–O3 and Li–O4) are very close to each other (~2.0 Å) and remain practically the same (Figure 4a). The fourth Li–O5 bond length increases by 0.3 Å with increasing temperature and the fifth $Li–O5^{iii}$ bond decreases by 0.25 Å and becomes almost to the same as the fourth one. Hence, the Li atom could be considered to be coordinated by three oxygen atoms at high temperature (Figures 3a and 4a).

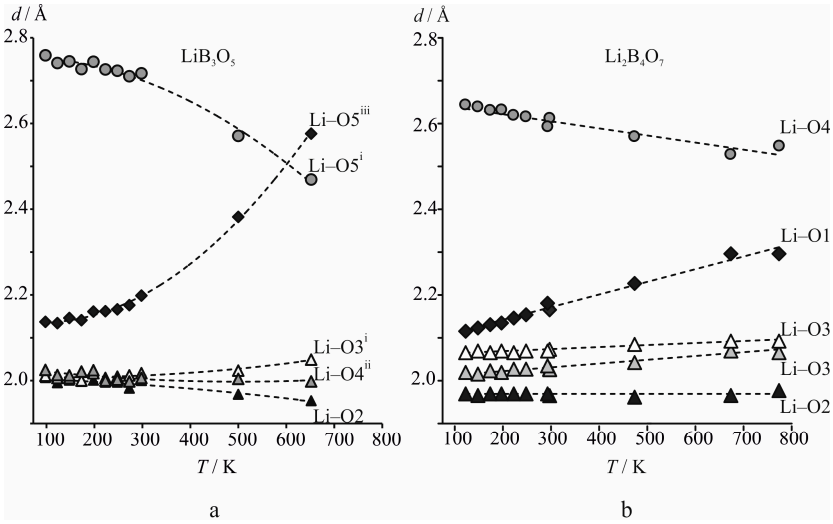

Figure 4. Temperature dependencies of Li–O bond lengths in LiB_3O_5 (**a**) ([47]; present work) and in $Li_2B_4O_7$ (**b**) after [51].

A similar situation occurs in $Li_2B_4O_7$: the LiO_4 tetrahedron at low temperatures [47] becomes an LiO_3 triangle at high temperatures (Figures 3b and 4b), although screw chains of LiO_5 polyhedra remain at a wide range of temperatures (Figure 5b). In the case of heavier and higher charges of Ba^{2+} in β-BaB_2O_4, the trend of decreasing of cation coordination number remains, although it is less distinctive (see Section 4.1).

Cations vibrations increasing. The isotropic displacements B_{eq} of the Li atoms increase more than four times upon heating to 377 °C. The anisotropy of Li thermal vibrations also increases. The elongation of the ellipsoid of thermal vibrations and the anharmonic figure lie near the *ac* plane and approximately under angles equal to *a* and *c* axis (Figures 3a and 5a). Li^+ cation thermal vibrations in $Li_2B_4O_7$ rapidly increase on heating to 773 K, the isotropic parameter B_{eq}(Li) increases by a factor of 2.5 [50,51]. The isotropic displacements U_{eq} of the Ba atom in β-BaB_2O_4 from 98 K to 650 K increases 5-fold (Table S16).

Thermal shifting of cations. As coordination number decreases under heating shifting of cations is observed [47,50,51]. For instance, in LiB_3O_5 the vibrational-active Li atom is displaced by 0.31 Å in the direction of the O2–O3–O4 plane upon heating from low temperatures to 377 °C (other atomic shifts are 0.04 Å on the average). In β-BaB_2O_4, the heavier Ba atom is moved towards screw 3_1 axis less significantly (see Section 4.1).

In LiB_3O_5 LiO_5 polyhedra linked by O5 atoms form chains within the channels, alternating with the chains of the triborate groups (see Section 4.2). At 500 K, Li moves 0.25 Å towards the O2O3O4 plane, and its coordination becomes triangular (d(Li–O) = 1.968–2.003 Å). The fourth $O5^{iii}$ oxygen that contributes to the tetrahedron at 20 °C moves away from Li (at a distance of 2.381 Å) and the fifth $O5^{i}$ oxygen is 2.6 Å away from Li (Figures 3a and 4a). At 650 K Li is clearly coordinated by three oxygen atoms, forming a planar LiO_3 triangle in the first coordination sphere, with two additional oxygen atoms on both sides of this triangle (second coordination sphere).

In $Li_2B_4O_7$ the Li atoms shift maximally (0.007 Å) along the *c* axis. The elongation of Li–O1 bonds by 0.115 Å leads to a removal of O1 from the first coordination sphere, whereas other bonds elongate by 0.006, 0.022, and 0.032 Å as shown by arrows in Figure 3b. The shift of the O1 atom leads to a highly irregular LiO_4 tetrahedron at high temperatures, almost a triangle like in LiB_3O_5.

Structural mechanism of thermal expansion. Lithium triborate, LiB_3O_5, demonstrates the maximum anisotropy of thermal expansion among all of the borates: $\alpha_a = 101$, $\alpha_b = 31$, $\alpha_c = -71 \times 10^{-6}$ K^{-1}. It can be seen that the difference of maximum and minimum values of the thermal expansion coefficients is 172 units [47]. At the same time, the thermal expansion coefficient of the volume ($\alpha_V = 60 \times 10^{-6}$ K^{-1}) equals the average for alkali metal borates.

The thermal expansion of the NLO borate $Li_2B_4O_7$ that contains tetraborate groups (see Table 2) is maximal in the *ab* plane ($\alpha_a = 16 \times 10^{-6}$ K^{-1}). Along the main axis, the *c* parameter shows compression ($\alpha_c < 0$) in negative and low temperature ranges (−180–250 °C) and expansion ($\alpha_c > 0$) at intermediate and high temperatures (250–750 °C) with the minimum ($\alpha_c = 0$) at about 250 °C. Here, we will try to explain the main features of this enigmatic thermal expansion. Structural studies [50,51] of $Li_2B_4O_7$ in a temperature range of −150 to 500 °C revealed considerable changes of the B1–O1–B2 angle between 4B-groups. They amount to about +2°, in contrast to the stability (0.1°) of the angles within the rigid 4B-groups.

As in the case of the unique framework of the triborate LiB_3O_5, the real reason for thermal deformations of the double interpenetrating boron–oxygen framework in $Li_2B_4O_7$ is the character of the thermal vibrations of the Li^+ cation. It is notable that in NLO Li borates the screw chains of LiO-polyhedra remain after conversion of LiO_4 into LiO_3 triangle [47,51]. It is notable that the screw chains of the LiO-polyhedra remain existent through the transformation of the LiO_4 tetrahedron into a LiO_3 triangle, as it is shown in the anharmonic approximation in LiB_3O_5 [47,51] and in $Li_2B_4O_7$ [51,54] (Figure 5).

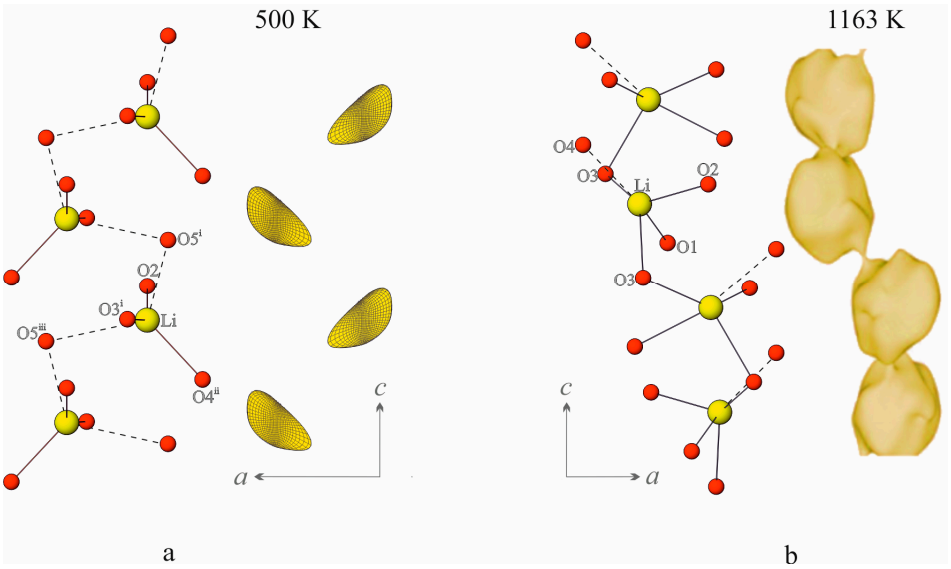

Figure 5. LiO_5 polyhedra chains along *c* axis in LiB_3O_5 (**a**) and $Li_2B_4O_7$ (**b**). The figures of thermal displacements of Li atoms are given in anharmonic approximation at 500 K in LiB_3O_5 (after [47]) while the nuclear scattering density maps are at 1163 K for $Li_2B_4O_7$ (after [54]). Symmetry codes for LiB_3O_5: (i) $-x + 1, -y + 1, z - 1/2$; (ii) $x - 1/2, -y + 3/2, z - 1$; (iii) $x, y, z - 1$.

The second-order NLO properties of LiB_3O_5, $CsLiB_6O_{10}$, and CsB_3O_5 borates, which all contain a topologically identical framework composed of 3B-groups, have been quantitatively studied from the viewpoint of the chemical bond [125]. It is noted that (i) differences in the NLO properties within this group of borates arise from the contributions of the different cations due to a changing coordination environment, i.e., the different interaction between the cation and the rigid anionic group; (ii) the $[B_3O_7]^{5-}$ group is very important for borate crystals. Heavier cations decrease the covalence values for the bonds in the anionic group and increase the susceptibility of the cation–oxygen bond. The latter, especially, leads to an increase in the resulting macroscopic susceptibility induced by the heavier cation. The present work shows that heavier cations strengthen the interaction between the cation and the $[B_3O_7]^{5-}$ anion.

3.3. Self-Assembly of Rigid Groups into NLO Borates

Anisotropic thermal vibrations of atoms could play a key role in the anisotropy of thermal expansion and in the self-assembly of rigid groups into crystal structure [26,43,45]. Here, we describe the self-assembly of BO_3 triangular radicals and mainly rigid groups containing BO_3 triangles into ordered crystal structures from the viewpoint of atomic thermal motion. The organizing force of self-assembly in borates is strong anisotropy of the thermal atomic vibrations in the BO_3 triangles, flat 3B- and other B–O rigid groups containing BO_3 triangles.

In the case of a BO_3 triangle (see Figure 1, 1B), O and B atoms oscillate mainly perpendicular to the strong B–O bond. There are three B–O bonds in the BO_3 triangle, thus B and O atoms maximally vibrate preferably perpendicular to the plane of an isolated BO_3 triangle (see Figure 1, 1B). The triangle as a whole has to vibrate to the direction perpendicular plane of the triangle. These triangles and rigid groups, due to the sharp anisotropy of thermal vibrations of B and O atoms, tend to be arranged in the parallel (or preferable) orientation. As a general trend [26,43,45], for NLO borates the self-assembly of rigid B–O groups containing triborate rings is characteristic in the process of crystal growth. Self-assembly is manifested in a parallel or preferred orientation of BO_3 triangles and 3B-rings. This is the cause of the high anisotropic thermal expansion of borate, which may contribute to the appearance of NLO properties in borates (see Table 2). Since most borates based upon asymmetric rigid BO_3 groups exhibit excellent NLO properties this has motivated in finding new NLO materials with other rigid TO_3 groups, such as carbonates and nitrates. In the most structures based upon isolated TO_3 triangles (T = B, C, N), TO_3 groups are represented in preferred orientation parallel to each other and the most of them show strong anisotropic thermal expansion [45]. Recently, for this reason carbonates have been widely studied, and a series of the materials have been discovered with proper NLO properties ([126], and Refs therein).

Most impressively, it is manifested in the case of a 3B-group composed of three triangles: internal B and O atoms vibrate maximally perpendicular to the plane of the triborate group (Figure 6a), and the whole group vibrates in the same direction. Hence a structure with isolated triborate groups has to expand considerably perpendicular to the plane of a group and expand weakly in parallel to the plane of a group (Figure 6c).

As an example, we can refer to the triborate group composed of three BO_3 triangles in comparison to the pole figure of thermal expansion of the crystal structure of β-BaB_2O_4 (Figure 6c), a crystal structure that is based on isolated triborate groups of three triangles 3B:<3Δ> (see Figure 1, n = 3). For β-BaB_2O_4 we also investigated the refractive indices (Figure 6b): N_g and N_p directions coincide to α_{min} and α_{max} [104], respectively. As seen from Figure 6 and other examples in [20], isolated triborate groups are usually arranged in parallel to each other to form 0D-3B structures, as seen in α- and β-BaB_2O_4 consisting of <3Δ> groups.

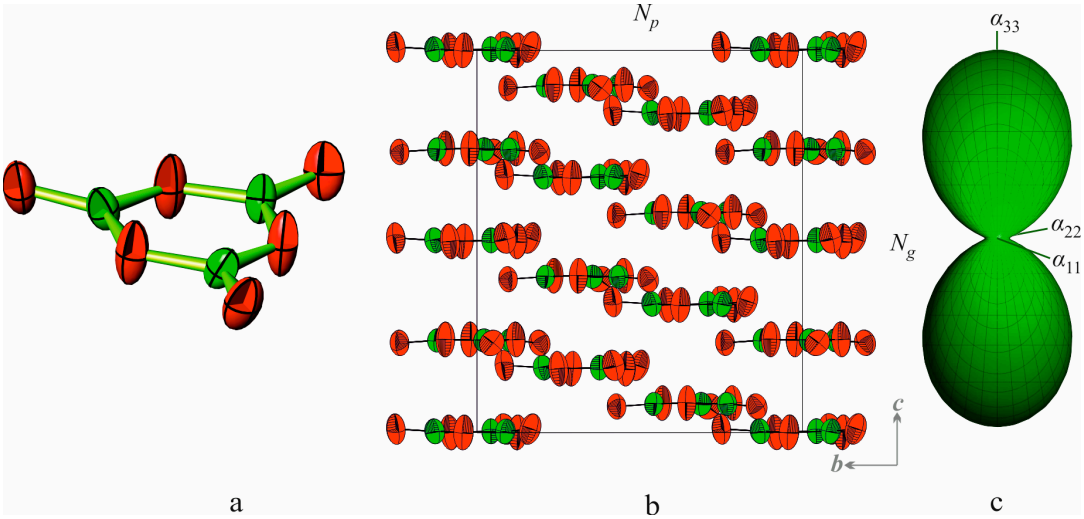

Figure 6. Self-assembly of (**a**) triborate groups to form crystal structures of zero-dimensionality (0D): (**b**) the β-BaB_2O_4 polymorph is based on <3Δ> rings in comparison to (**c**) pole figure of thermal expansion (after [45]).

3.4. Strong Anisotropy of the Thermal Expansion in NLO Borates

For most borates a high anisotropy of the thermal expansion is characteristic, as has been found in [26,34,42]. It can be analysed to serve as an additional criterion for NLO borates, like high values of $n_g - n_p$ birefringence [12,15], etc. Similarly, we evaluated the degree of the anisotropy of thermal expansion by a value $\Delta = \alpha_{max} - \alpha_{min}$ (Table 2). Non-centrosymmetric as well as NLO borates often show stronger anisotropy of thermal expansion in comparison to centrosymmetric borates of the same group. For example, among Ba borates β-BaB_2O_4 ($\Delta = 42 \times 10^{-6}$ K^{-1}) is featured with the most anisotropy, among bismuth borates—α-BiB_3O_6 ($\Delta = 82 \times 10^{-6}$ K^{-1}), and among lithium borates—LiB_3O_5 ($\Delta = 172 \times 10^{-6}$ K^{-1}) is the evident record-breaker. However, there are exceptions as for any semi-empirical rule. So, among K-borates the centrosymmetric polymorph β-KB_5O_8 ($\Delta = 63 \times 10^{-6}$ K^{-1}) shows the highest anisotropy whilst NLO $K[B_5O_6(OH)_4]\cdot 2H_2O$ ($\Delta = 37 \times 10^{-6}$ K^{-1})—lower anisotropy. Among caesium borates the nonlinear-optical compound CsB_3O_5 shows relatively low anisotropy of the thermal expansion ($\Delta = 25 \times 10^{-6}$ K^{-1}), while other caesium borates expand more anisotropically. It should be noted that among rubidium borates the non-centrosymmetric polymorphs α- and β-RbB_3O_5 ($\Delta = (91–100) \times 10^{-6}$ K^{-1}) show the highest anisotropy of expansion; however, their NLO properties are not known. However, a record anisotropy of thermal expansion among the rubidium borates of both non-centrosymmetric (α- and β-) polymorphs RbB_3O_5 ((91–100) $\times 10^{-6}$ K^{-1}) leads us to expect that at least one of them generates a significant second harmonic.

It is remarkable that the non-centrosymmetric borate SrB_4O_7 borate expands almost isotropically. As noted by Becker [35], the birefringence of this borate and the isostructural PbB_4O_7 are inconsiderable, and as a consequence phase matching is not possible. Reasons for the occurrence of strong anisotropy are discussed in [44]. The reasons for a manifestation of high anisotropy of NLO borates in comparison to centrosymmetric borates are discussed in the next Section 3.5.

3.5. Reasons for Strong Anisotropy of the Thermal Expansion of Borates

Borates exhibit thermal expansion that are strongly anisotropic and appear to be maximal for those compounds that contain isolated BO_3 triangles or rigid boron–oxygen groups and unfixed lattice angles (monoclinic and triclinic crystals).

The B and O atoms in planar, triangular 3B-groups vibrate maximally along the normal to the plane of the triangle, and minimally in the plane itself, generating maximal and minimal expansion, respectively.

As it was shown in Section 2.2.3, rigid groups almost do not change their size and configuration with temperature and adjust themselves to variable temperatures only by mutual rotation around shared oxygen atoms. This large hinge mechanism is strongly anisotropic by virtue of its nature.

The question can arise, why such anisotropy of structural (in particular thermal) deformations is characteristic for borates but not to the same extent for silicates, for example? The answer is simple—there are almost no unalterable atomic groups in silicates, such as rigid boron–oxygen groups; only the SiO_4 tetrahedra are unalterable with temperature, but larger polyanions (pyroxene chains, amphibole ribbons, tetrahedral nets, etc.) are not rigid, i.e., they have internal degrees of freedom for reconstruction to reach an energy minimum. However, silicates exhibit a strong anisotropy of thermal expansion by another mechanism—for oblique angle (monoclinic and triclinic) crystals by way of shears ([43], and Refs therein) connected to changes of angular lattice parameters. Shears are definitely characteristic of borates, too.

Thus, the manifestation of a strong anisotropy of the thermal deformation of crystals has at least three main reasons [44]: (1) shears, or shear deformations, which are characterised by changes of angular lattice parameters; (2) strong anisotropy of atomic thermal vibrations in planar anionic groups (TO_3 triangles); (3) hinges, or deformations of an assembly of corner-sharing rigid groups, having no own (internal) degrees of freedom to adjust themselves to varying thermodynamic conditions (T, p, X). The first of the reasons listed above can be realized in silicates, the first and the second in carbonates, and all the three reasons are realized in borates. That is why borates most often demonstrate a thermal expansion that is strongly anisotropic. It can be assumed that this is characteristic not only for thermal deformations, but also for pressure, composition (chemical) and other types of crystal structure deformations. In all cases, rigid boron–oxygen groups make a decisive contribution to the sharp anisotropy of the structural deformations of borates. For this reason, we will clarify this concept.

3.6. "Rigidity" of Rigid Groups

At ambient conditions BO_3 triangles and BO_4 tetrahedra demonstrate systematic variations of bond lengths and angles, i.e., (a) the average <B—O> bond length is 1.37 Å for triangles and 1.47 Å for tetrahedra; (b) approximately the same values are characteristic of terminal <B—O> bonds; (c) regular variations of the bridging B—O bonds $<B^{\square}–^{\square}O^{A}> > <B^{\square}–^{\square}O^{\square}> > <B^{A}–^{A}O^{A}> > <B^{A}–^{A}O^{\square}>$ and so on are caused by various environments of O and B atoms [34]. Under high pressure, the number of BO_4 tetrahedra and edge-sharing (O–O) tetrahedra increases [63–65].

An earlier review [26] the results on single crystal HTXRD and LTXRD studies were summarized for more than ten borate structures as well as high-temperature powder X-ray diffraction data for about 70 borates. These studies allow to formulate the following basic principles of high-temperature borate crystal chemistry. *On heating, BO_3 and BO_4 polyhedra and rigid groups consisting of these polyhedra, maintain their configuration and size (accurate to the vibrations amplitudes), i.e., they are thermally rigid. But rigid groups are able to rotate like hinges exhibiting thermal expansion that is highly anisotropical, including negative linear expansion.*

As it has been noted in [26], the thermal invariability of groups means that changes in the rigid groups do not exceed the error bars of 0.003 Å for average bond lengths and of 0.5° for B–O–B bond angles. This holds for the temperature range of 20 to 500 °C.

Angles between rigid groups can vary over a wider range from about 2° to 4° for the same temperature range. Within groups considered as non-rigid ones, the changes in bond angles are similar to those in between rigid groups.

Thus, in [26] the temperature dependence analysis of B–O bond lengths and B–O–B bond angles was presented for a characteristic thermal behaviour of rigid boron–oxygen groups; however, changes of the O–O–O angles with temperature were left without attention.

Now, the experimental data from [26] were used for additional calculations on the O–O–O angles at different temperatures. The results of these calculations are represented in Figure 7 for different types of B–O groups. Values of the changes of the O–O–O angles are given for each group

in a specified temperature range. If such changes do not exceed the measurement error (0.5°), then the value of the change of the angle is not specified in the figure.

It is seen from Figure 7 that the O–O–O inner angle (inside the rigid group) almost does not change with temperature. Changes of the outer angles (along the perimeter of a rigid group) exceed the measurement errors and can reach a few degrees.

Let us return to the understanding of the "thermal rigidity" term of the rigid group. The authors of [26] understand it as follows: *"Average B–O bond lengths change in triangles and tetrahedra in the temperature range 20–500 °C usually do not exceed the error bars 0.003 Å." "Variations of B–O–B angles within rigid boron–oxygen groups usually are equal or less than 0.5° at least in the temperature range of 20–500 °C. This value is comparable with the error bars. Angles between rigid groups can vary in wider range (about 2°) at the same temperatures. Within groups considered as non-rigid ones, the changes in bond angles are similar to those in-between rigid groups"*.

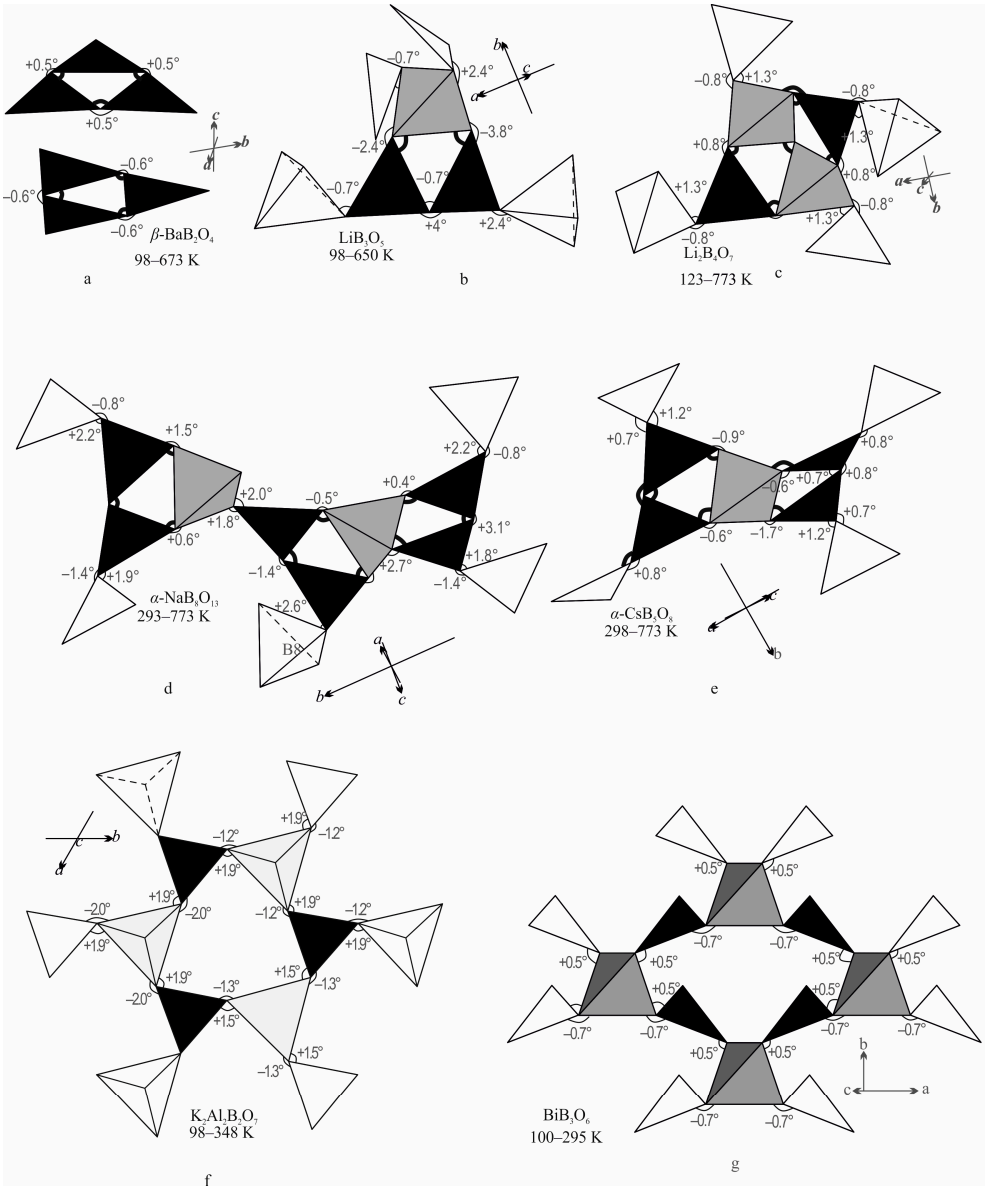

Figure 7. Changes of the O–O–O angles of boron–oxygen groups in the structures of (**a**) β-BaB_2O_4; (**b**) LiB_3O_5; (**c**) $Li_2B_4O_7$; (**d**) α-CsB_5O_8; (**e**) α-NaB_8O_{13}; (**f**) BiB_3O_6; (**g**) $K_2Al_2B_2O_7$. Inner angles change less than 0.5° in rigid groups (**a**–**e**); they are shown by a bold line with no numbers.

Now, after calculation of the O–O–O angles, it is possible to give a more generalized definition: the thermal invariability of the rigid group means that the lengths and bond angles of the rigid

group remain almost unchanged when the temperature changes (angles O–O–O are not the bonds angles).

4. New Temperature-Dependent Structural Studies of NLO Borates from Single-Crystal LTXRD and HTXRD Data

As it was mentioned in the introduction, this review also contains new experimental data on NLO borates. Here we represent our findings on the crystal structures of β- and α-BaB_2O_4, LiB_3O_5 as well as $K_2Al_2B_2O_7$, which were obtained from single crystal X-ray diffraction data for a wide range of temperatures.

4.1. β-BaB_2O_4 (98, 123, 173, 223, 295, 323, 693 K) and α-BaB_2O_4 (295, 673 K)

This barium borate allows it to compare the crystal structures and thermal deformations of a NLO and a LO phase of the same chemical composition. Both modifications are based on the same isolated groups. For the first time, the crystal structure of β-BaB_2O_4 was described in [127]. Afterwards it was refined at different temperatures [49]. At the same time, the crystal structure of HT modification of α-BaB_2O_4 was published [60], with the parameters of the thermal displacement of atoms adjusted using an isotropic approximation. Both modifications crystallize in the trigonal system, the space groups are *R*3*c* for β-BaB_2O_4 and *R*-3*c* for α-BaB_2O_4. The borate anion of both polymorphs is characterized by isolated cyclic 3B-groups of three BO_3, 3B:3Δ:<3Δ> (see Figure 1). A review on single-crystal growth, properties and crystal structures of the polymorphs of BaB_2O_4 was given in [128]. Previously [104], we examined the thermal expansion of β-BaB_2O_4 by powder HTXRD methods, and found it to be strongly anisotropic, similar to the thermal expansion of α-BaB_2O_4 briefly presented in [26,38,43]. Here we present data on the crystal structures of β-BaB_2O_4 and α-BaB_2O_4, determined by single-crystal X-ray diffraction data in the temperature ranges of 98–673 K and 298–694 K, respectively.

The temperature dependence of the cell parameters (Figure 8) was described for β- and α-BaB_2O_4 by first-order polynomials, like in [38]. Figures of the tensor of the thermal expansion versus the structure are shown in Figure 9. The anisotropy of the expansion is dictated by the orientation of rigid 3B-groups in the structure, where expansion in the plane is minimal and perpendicular to the plane is maximal. The comparison between both modifications (Figures 8 and 9) shows, that the nonlinear-optical polymorph expands more anisotropically ($\alpha_{11} = \alpha_a = 3$, $\alpha_{33} = \alpha_c = 45 \times 10^{-6}$ K^{-1}) than the centrosymmetric phase, α-BaB_2O_4 ($\alpha_a = 6$, $\alpha_c = 28 \times 10^{-6}$ K^{-1}), although their volumetric expansion is comparable: $\alpha_V = 40$ and 51×10^{-6} K^{-1} for β and α-BaB_2O_4.

The examination of the crystal structures of both modifications, β- and α-BaB_2O_4, over a wide range of temperatures (98–673 and 298–694 K, respectively) shows also the difference in thermal transformations of the structure. In the β-BaB_2O_4 structure, the Ba atom occupies a general position *6b*, where it is coordinated by eight oxygen atoms at distances of 2.643(4), 2.708(4), 2.766(5), 2.781(5), 2.837(4), 2.828(6), 2.906(4) and 3.058(5) Å (at 298 K). Temperature dependencies of Ba–O bond lengths are shown in Figure 10a. The thermal expansion coefficients of these bond lengths are 12, −1, 21, 7, 40, −11, 6 and 35×10^{-6} K^{-1}, respectively.

In α-BaB_2O_4 the Ba atoms occupy two special positions, 6*a* and 12*c*, where they are coordinated by a regular trigonal prism (bond length 2.66(3) Å × 6 at 298 K) and by nine oxygen atoms (2.74(1) Å × 3, 2.83(3) Å × 3, 3.08(1) Å × 3). Temperature dependencies of Ba–O bond lengths are shown in Figure 10b. The thermal expansion coefficients of these Ba–O bond lengths in the BaO_9 polyhedron are 3, 28 and 23×10^{-6} K^{-1}, and in the BaO_6 polyhedron they are 19×10^{-6} K^{-1}.

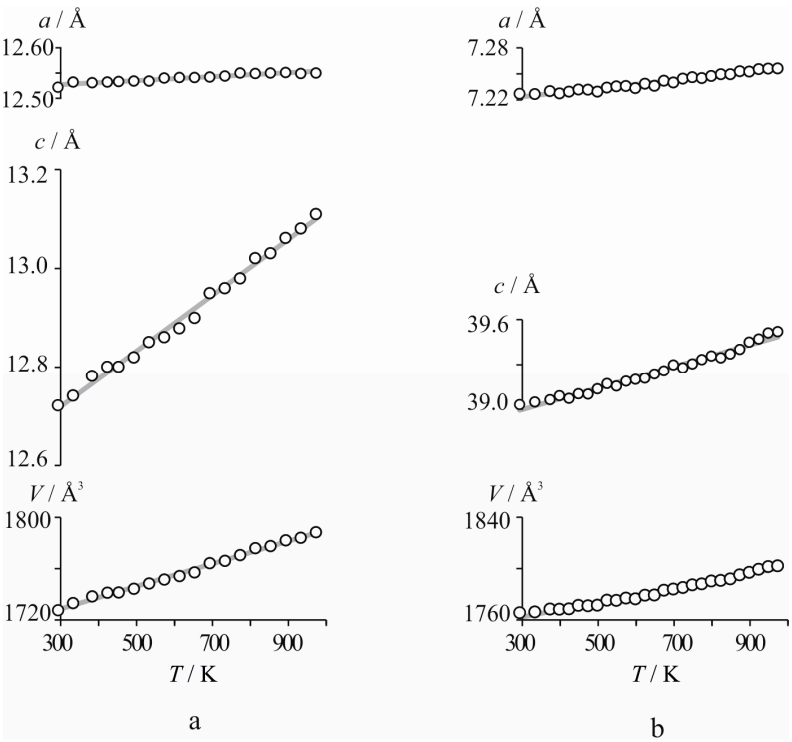

Figure 8. Temperature dependence of lattice parameters and the volumes of the unit cells of β-BaB_2O_4 (**a**) and α-BaB_2O_4 (**b**).

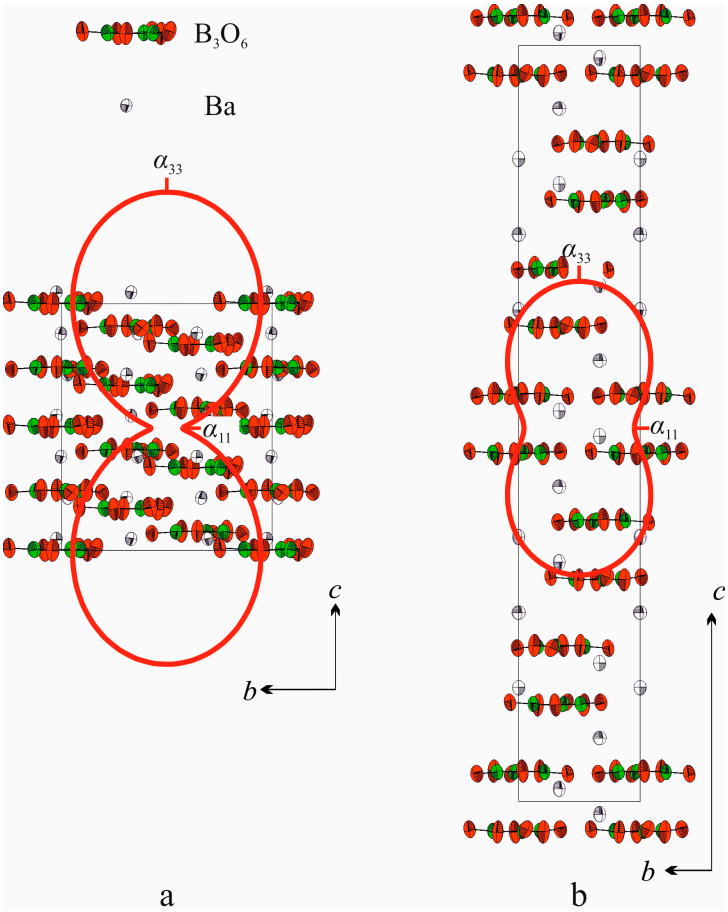

Figure 9. Crystal structures of (**a**) β-BaB_2O_4 [104] and (**b**) α-BaB_2O_4 versus the pole figures of the coefficients of thermal expansion.

Thermal deformations of the crystal structure of β-BaB_2O_4 are considerably more anisotropic compared to those of α-BaB_2O_4, and they show themselves mainly in the coordination sphere of barium. A thermal change that is strongly anisotropic leads to a shift of Ba in the BaO_8 polyhedron in β-BaB_2O_4 by a considerable value 0.035 Å along the direction of the 3_1 screw axis (Figure 10c). These changes in the coordination sphere are followed by an anharmonicity of the vibrations of Ba, although inconsiderable (see Figure 3c).

Lengths and angles of the bonds in the 3B-groups of β-BaB_2O_4 are almost stable upon temperature changes. In the 3B-groups, the B–O bond lengths of the bridging oxygen atoms (1.393(9)–1.415(7) Å for β-BaB_2O_4 and 1.42(2) Å for α-BaB_2O_4 at 298 K) are longer than for the apical ones (1.329(10), 1.323(11) for β-BaB_2O_4 and 1.39(1) Å for α-BaB_2O_4 at 298 K). This is related to the fact that the terminating O atom is linked with one B atom, while the bridging O atom is linked with two boron atoms. As a result, the related bridging B–O bond is weaker and longer than for the terminal B–O bonds, which is in accordance to analogous observations in other borates [26]. Individual B–O bond lengths as a function of temperature are given in Figure 2a.

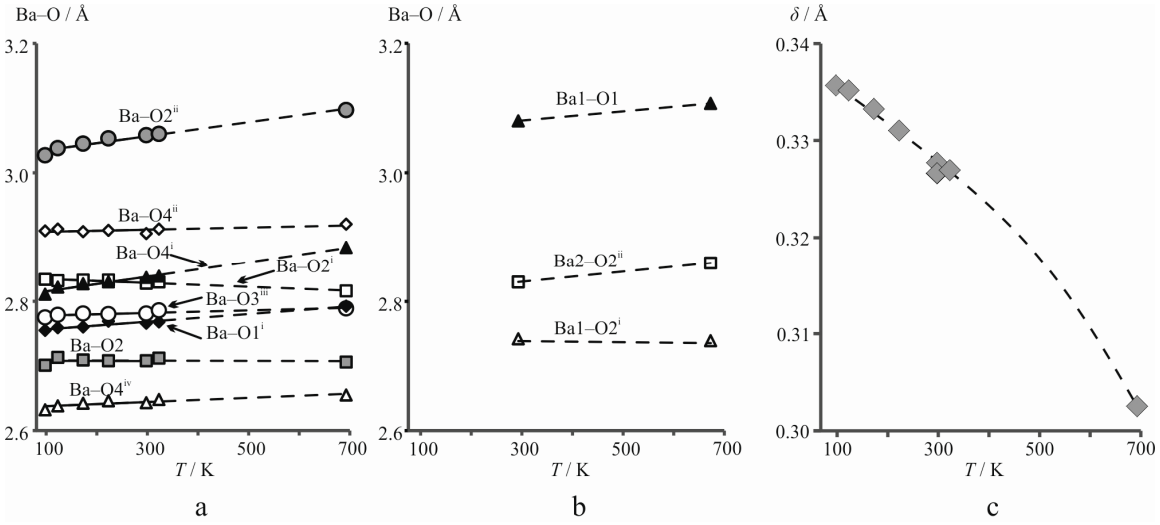

Figure 10. Temperature dependences of Ba–O bond lengths in the structures of (**a**) β-BaB_2O_4 and (**b**) α-BaB_2O_4; (**c**) Distance from barium atom to the screw 3_1 axis versus temperature. Symmetry code(s) for β-BaB_2O_4: (i) $-y + 2/3, -x + 1/3, z - 1/6$; (ii) $-x + y + 1/3, -x + 2/3, z - 1/3$; (iii) $-y + 1/3, -x + 2/3, z + 7/6$; (iv) $-x + y, y, z - 1/2$. Symmetry code(s) for α-BaB_2O_4: (i) $x + 1/3, y + 2/3, z - 1/3$; (ii) $-y - 2/3, x - y - 1/3, z - 1/3$.

4.2. LiB_3O_5 (98, 123, 148, 173, 198, 223, 248, 273, 298, 293, 500, 650 K)

Lithium triborate exhibits excellent nonlinear optical properties paralleled by a high threshold for laser damage, which is required for many applications. The compound crystallizes orthorhombically, space group *Pna*2_1. The crystal structure of this well-known NLO borate was solved at room temperature [128–130] and then refined, with special attention to the distribution of the electron density [124,131]. The structure consists of a framework of <2Δ□> 3B-rings consisting of two triangles and a tetrahedron (Figure 7b), and Li atoms located in the interspaces of this framework. Its peculiarity is a thermal expansion anisotropy that is extreme amongst borates (α_a = 101, α_b = 31, α_c = −71 × 10^{-6} K^{-1}), with significant values of the coefficients of anharmonic approximation for the Li atoms (see Sections 3.1 and 3.2), high mobility and dramatic shifts of Li of 0.26 Å [47].

Upon heating from 98 to 650 K the Li atoms show an increase of the amplitudes of their vibrations, that is accompanied by anharmonicity of its vibrations, as shown by us [47]. Furthermore, the coordination number of lithium decreased from four to three. This was described in detail in Section 3.2. The thermal mobility of the lithium atoms is reflected in the changes of the boron–oxygen framework, which is compressed along the *c* axis and expands along the *a* and *b axes*. Within the boron–oxygen groups the B–O bonds lengths and angles remain (in the limit of error)

almost unchanged (see Figure 2b). A slight contraction of the B–O bond lengths was corrected in the view of atomic thermal vibrations, so that the rigid 3B-groups in LiB_3O_5 did not change in configuration or size on heating, but they rotated relatively to each other. The plane of the 3B-group is considered to be the plane outlined through the boron atoms. In the rigid triborate the corner-shared groups are condensed to form screw chains around the 2_1 axis (Figure 11). Upon heating from 98 up to 650 K the angle between the planes of adjacent 3B-groups changed for more than 3°, and the correspondent B–O–B angle changed for 3.8°. Thus, the B–O screw chain is changed like a hinge: it contracts along the *c*-axis and expands in direction of the *a*-axis.

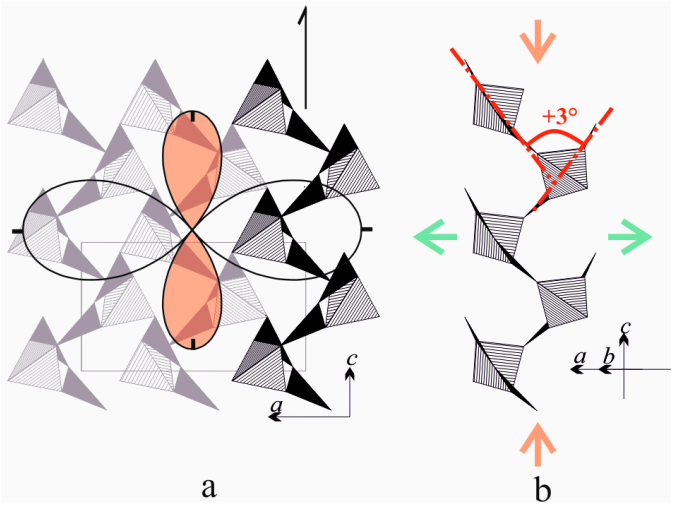

Figure 11. Crystal structure of LiB_3O_5 versus the pole figure of the coefficients of the thermal expansion (**a**). The sharp anisotropy of the thermal expansion is caused by the contraction of the chain of 3B-groups. Upon heating from 98 up to 650 K the angle between planes of adjacent 3B-groups is changed for more than 3° (**b**).

4.3. $K_2Al_2B_2O_7$ (98, 123, 173, 223, 298, 348 K)

The crystal structure of $K_2Al_2B_2O_7$ is trigonal, with space group *P*321 [21,132–134]. The structure contains a framework built of corner-sharing tetrahedra of AlO_4 and triangles of BO_3. Triangles and tetrahedra form six-fold rings of three AlO_4 tetrahedra parallel to the *ab* plane. They alternate with three BO_3 triangles, resulting in the general formula $Al_3B_3O_{12}$ (Figure 12a). Planes of triangles are almost parallel to the *ab* plane, while two AlO_4 tetrahedra of each ring are directed towards one side and one tetrahedron towards the opposite side. Layers of rings are polymerized to form a framework through the corners of aluminium–oxygen tetrahedra (Figure 12b).

We examined the crystal structure of this borate at 98, 123, 173, 223, 298, and 348 K. According to [85], the thermal expansion is less anisotropic compared to other borates: $\alpha_a = 8$, $\alpha_c = 16 \times 10^{-6}$ K^{-1}. Consisting of rigid BO_3 triangles and AlO_4 tetrahedra, the six-membered boron–aluminate ring is not rigid and—upon heating—is subject to considerable thermal rearrangements (see Section 3.6). B–O–Al angles inside the ring are 156° and 84°, however, between 98 and 348 K they change about +1.5°–1.9° and −1.2°–2.0°, respectively. Thus, the boroaluminate ring changes considerably in the *ab* plane; however, adjacent rings align their thermal deformations to the result, that the expansion in the *ab* plane becomes inconsiderable. With a rise in temperature the ring turns into a more regular shape, and the planes of the BO_3 triangles are parallel to the *ab* plane. A decrease of the angle between the BO_3 triangles and the *ab* plane can be the reason for the strong expansion along the *c* axis.

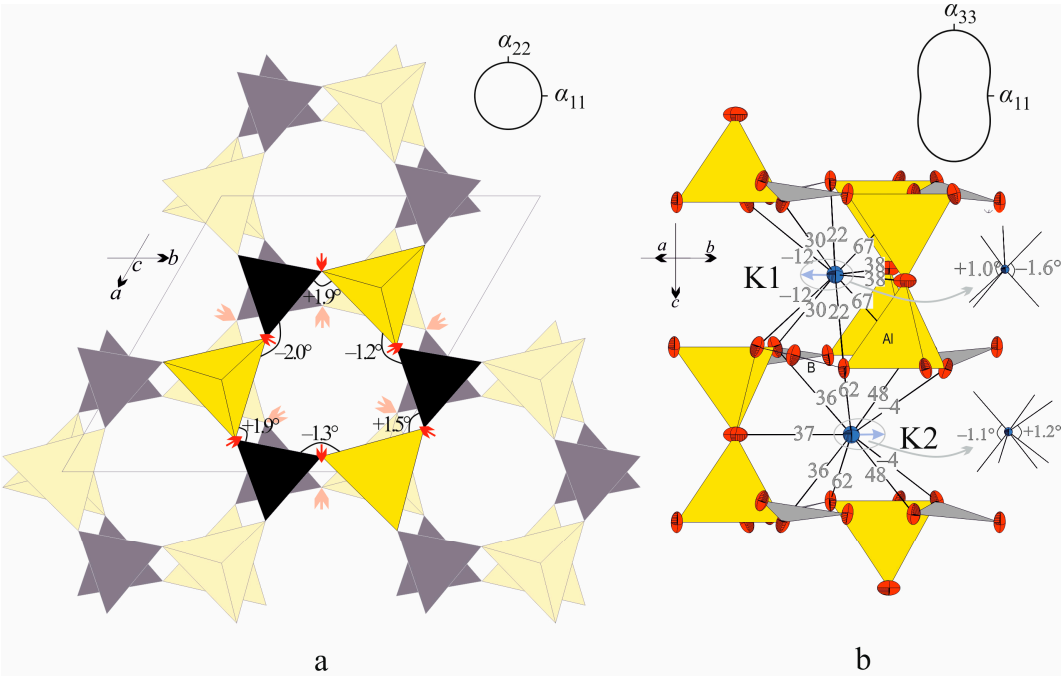

Figure 12. Projections of the crystal structure of $K_2Al_2B_2O_7$ onto (**a**) *ab* and (**b**) *bc* planes versus the pole figures of thermal expansion coefficients. Changes of O–O–O angles in between polyhedra are shown on (**a**). Next to the K–O bonds in (**b**) are shown their coefficients of thermal expansion ($\times 10^{-6}$ K^{-1}).

Considerable changes of the B–O–Al angles within the hexagonal ring are followed by significant transformations of the coordination sphere of potassium. Potassium atoms occupy two special positions K1 and K2, where they are coordinated by ten and nine atoms of oxygen at distances of 2.680(3) × 2, 2.954(1) × 2, 3.020(3) × 2, 3.198(2) × 2, 3.344(3) × 2 Å and 2.679(2) × 2, 2.751(3) × 2, 3.058(1), 3.212(3) × 2, 3.252(3) × 2 Å, respectively. Coefficients of the thermal expansion for these K–O bonds are 30 × 2, 38 × 2, 67 × 2, 22 × 2, −12 × 2 10^{-6} K^{-1} and 62 × 2, 48 × 2, 37, 36 × 2, −4 × 2 10^{-6} K^{-1}, respectively. The temperature dependence of the K–O bonds lengths are shown in Figure 13. Analyzing the distribution of these bond lengths, it is easy to note that the thermal expansion coefficients are greater in one hemisphere (for example, 38 × 2 and 67 × 2 10^{-6} K^{-1} for K1) than in the other (30 × 2 and −12 × 2 10^{-6} K^{-1} for K1). This is connected to the temperature-induced displacements of the potassium cations relative to the boron–aluminate framework. Thus, rather considerable changes happen in the coordination sphere of potassium, and its coordination polyhedron varies anisotropically with temperature increasing.

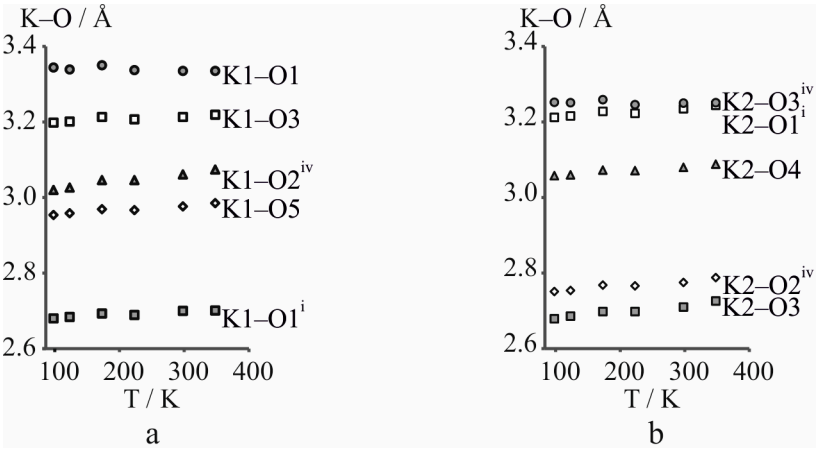

Figure 13. Temperature dependences of (**a**) K1–O and (**b**) K2–O bond lengths in the structure of $K_2Al_2B_2O_7$. Symmetry codes: (i) $-x + y, -x, z$; (ii) $y, x, -z$; (iii) $x - y, -y, -z$; (iv) $-y + 1, x - y, z$; (v) $-x + 1, -x + y, -z$; (vi) $y, x - 1, -z$; (vii) $y, x, -z + 1$; (viii) $-x + 1, -x + y, -z + 1$; (ix) $x - y, -y, -z + 1$.

5. Materials and Methods

Experimental approaches and techniques. Single crystals of β-, α-BaB_2O_4 and $K_2Al_2B_2O_7$ were grown by the TSSG method described in [135–137], while the crystals of LiB_3O_5 were obtained by cooling from a melt as described in [47]. Optically clear single crystals of suitable quality for X-ray diffraction were selected using a polarizing microscope, and mounted on a glass fibre. The crystals of β-BaB_2O_4 (98, 123, 173, 223, 295, 323 K), LiB_3O_5 (98, 123, 148, 173, 198, 223, 248, 273, 298 K) and $K_2Al_2B_2O_7$ (98, 123, 173, 223, 298, 348 K) were measured using STOE IPDS II diffractometer, graphite-monochromated MoKα-radiation, frame widths of 1° in ω. A hot/cold air blower (Oxford Cryosystems, Oxford, UK) was used for temperature control.

High-temperature measurements on β-BaB_2O_4 (298, 693 K) and α-BaB_2O_4 (298, 673 K) were performed using an automatic three-circle diffractometer installed at the Institute of Silicate Chemistry of Russian Academy of Sciences (inventors—Prof. Yurij F. Shepelev and Prof. Yurij. I. Smolin; software development—Prof. Yurij F. Shepelev and Dr. Alexander. A. Levin) with the perpendicular beam scheme using graphite-monochromatised MoKα-radiation. The crystal placed on a glass capillary by a special high-temperature glue was blown with hot air while being measured. To study the anharmonicity of atomic vibration, the crystal of β-BaB_2O_4 was measured at room temperature with $(\sin\theta/\lambda)_{max}$ = 1.03 using a Bruker Smart APEX II diffractometer (Bruker, Billerica, MA, USA).

The data were corrected for Lorentz, polarization, absorption, and background effects. The sample of $K_2Al_2B_2O_7$ was twinned with (−1, 0, 0, 0, −1, 0, 0, 0, 1) twinning matrix and a ~1:3 twin domains ratio. The structures were refined starting from the positional parameters of LiB_3O_5 [47] and $K_2Al_2B_2O_7$ [134]. Crystal structures of β- and α-BaB_2O_4 were solved using Shelx-97 software (Göttingen, Germany) [138] and refined with JANA2006 software [139]. The joint-probability density function was calculated from the inverse Fourier transform of the anharmonic ADPs approximated by the third- and fourth-order expansion of the Gram–Charlier series [140]. Anharmonic temperature factors (C_{ijk}) of the third order for oxygen and boron atoms appeared to be of the same order as their ESDs. C_{ijk} and D_{ijkl} coefficients were significant (more than 3σ) only for Ba atoms (see Table S4). Data visualization was performed with the Vesta software (Tsukuba, Japan) [141]. Experimental details, refinement results, final atomic positional and displacement parameters, selected bond lengths and angles for β-BaB_2O_4, α-BaB_2O_4, LiB_3O_5 and $K_2Al_2B_2O_7$ are given in Tables S1–S8, S9–S14, S15–S21 and S22–S28, respectively.

CCDC 1531519–1531543 contains the supplementary crystallographic data for this paper. These data can be obtained free of charge via http://www.ccdc.cam.ac.uk/conts/retrieving.html (or from the CCDC, 12 Union Road, Cambridge CB2 1EZ, UK; Fax: +44-1223-336033; E-mail: deposit@ccdc.cam.ac.uk).

Thermal expansion of α-BaB_2O_4 was studied in air by means of a Stoe Stadi P X-ray diffractometer with CuKα radiation (Darmstadt, Germany) with a high-temperature camera Büchler HDK S1 (Hechingen, Germany). The sample was prepared on a Pt–Rh plate using a suspension in heptane. The temperature step was 40 K in the range 293–373 K and 25 K in the range of 373–973 K. Unit-cell parameters of the compound at different temperatures were refined by the least-squares method. Main coefficients of the thermal expansion tensor were determined using a polynomial approximation of temperature dependencies for the unit-cell parameters by ThetaToTensor program (Institute of Silicate Chemistry of Russian Academy of Sciences, Saint-Petersburg, Russia) [142].

6. Conclusions

There is growing evidence that the NLO properties of a material are related to the particular features of its atomic molecular structure. In this context, there is a good reason to investigate the relationship between the crystal structure and the NLO properties of borates. The most common group in the NLO borates are isolated BO_3 triangles, followed by single 3B-rings and double cyclic 4B- and 5B-groups, composed of 3B-rings; other groups are scarce.

The BO_3 triangles and the cyclic 3B-groups are flat and asymmetrical in shape. Hence, we conclude that the asymmetrical flat shape of anionic groups is strongly preferred in NLO borates. A

flat shape of the anionic groups leads to their preferable arrangement in parallel to each other, i.e., to the self-assembly of a drastically anisometric crystal structure of NLO borates.

The anisometric atomic molecular structure of NLO borates generally gives rise to a pronounced anisotropy of their physical properties, and thermal expansion follows this trend. It was noted that the sharp anisotropy of thermal expansion is common for borates that have a pseudo-layered structure. In this review, we show (see Table 2) that the borates generating the second harmonic exhibit stronger anisotropy of thermal expansion.

The sizable birefringence, mentioned in Section 4.3, is an example of a physical property that is governed by the "layered" structure of borates. Indeed, a pronounced anisotropy of physical properties ensues from the preferred orientation of BO_3 triangles and 3B-rings comprising such triangles. The "layers" are characterized by the highest density, the slowest propagation of light oscillating in the plane of the layer, thus the highest refractive index n_g. In contrast, the direction perpendicular to the layers has the minimal density, the fastest propagation of the waves oscillating in this plane, while the refractive index n_p reaches its minimal value. This gives rise to the sizable birefringence $n_g - n_p$.

Since the birefringence and the anisotropy of thermal expansion are functions of the same argument (pseudo-layered structure), the significant birefringence correlates with the high anisotropy of thermal expansion: n_g corresponds to α_{min}, $n_p - \alpha_{max}$. The borate β-BaB_2O_4 (see Figure 6, $n_g - n_p = 0.041$) is a typical example. In this respect, high anisotropy can be considered a further criterion for NLO borates. In particular, by analysing the thermal expansion tensor of two dozen non-centrosymmetric borates versus their centrosymmetric counterparts (see Table 2), we demonstrated that most NLO borates exhibit a pronounced anisotropy of thermal expansion. In turn, the reason for the anisotropy of thermal expansion is the thermal vibrations of atoms.

As noted by Chen and co-authors, the anionic groups are primarily responsible for the second harmonic generation, although the cationic contributions cannot be neglected. We can conclude that the thermal mobility of cations rises significantly: their anharmonic components of thermal vibrations increase a few times to reach significant values, the cations shift, and, as a result, the coordination number of cations tends to decrease with temperature. The mobility of cations in centrosymmetric structures is less pronounced than in non-centrosymmetric ones.

Supplementary Materials: The following are available online at www.mdpi.com/2073-4352/7/3/92/s1, Figure S1: Changing of O–O distances and O–O–O in boron–oxygen groups in structures (a) β-BaB_2O_4, (b) LiB_3O_5, (c) $K_2Al_2B_2O_7$, Table S1: E*x*perimental details of β-BaB_2O_4 measurements, Table S2: Atomic coordinates, displacement parameters (Å^2) and site-occupanc*y* factors (SOFs) in the structure of β-BaB_2O_4 modifications at different temperatures, Table S3: Anisotropic parameters of atomic displacements in β-BaB_2O_4 at different temperatures, Table S4: Anharmonic thermal parameters (× 10^{-4}) of the third and fourth order for barium atoms in the structure of β-BaB_2O_4 at 298 K obtained using the Gram–Charlier model, Table S5: B–O (Å) bond lengths and O–B–O (°) angles in the β-BaB_2O_4 structure at different temperatures, Table S6: Ba–O (Å) bond lengths and O–Ba–O (°) angles in the β-BaB_2O_4 structure at different temperatures, Table S7: B–O–B (°) angles in the β-BaB_2O_4 structure at different temperatures, Table S8: O–O–O (°) angles in the β-BaB_2O_4 structure at different temperatures, Table S9: E*x*perimental details of α-BaB_2O_4 measurements, Table S10: Atomic coordinates displacement parameters (Å^2) and site-occupanc*y* factors (SOFs) in the structure of α-BaB_2O_4 modifications at different temperatures, Table S11: Anisotropic parameters of atomic displacements in α-BaB_2O_4 at different temperatures, Table S12: B–O (Å) bond lengths and O–B–O (°) angles in the α-BaB_2O_4 structure at different temperatures, Table S13: Ba–O (Å) bond lengths and O–Ba–O (°) angles in the α-BaB_2O_4 structure at different temperatures, Table S14: O–O–O (°) angles in the α-BaB_2O_4 structure at different temperatures, Table S15: E*x*perimental details of LiB_3O_5 measurements, Table S16: Atomic coordinates, displacement parameters (Å^2) and site-occupanc*y* factors (SOFs) in the structure of LiB_3O_5 at different temperatures, Table S17: Anisotropic parameters of atomic displacements in LiB_3O_5 at different temperatures, Table S18: Li–O (Å) bond lengths and O–Li–O (°) angles in the LiB_3O_5 structure at different temperatures, Table S19: B–O (Å) bond lengths and O–B–O (°) angles in the LiB_3O_5 structure at different temperatures, Table S20: B–O–B (°) angles in the LiB_3O_5 structure at different temperatures, Table S21: O–O–O (°) angles in the LiB_3O_5 structure at different temperatures, Table S22: E*x*perimental details of $K_2Al_2B_2O_7$ measurements, Table S23: Atomic coordinates, displacement parameters (Å^2) and site-occupanc*y* factors (SOFs) in the structure of $K_2Al_2B_2O_7$ at different temperatures, Table S24: Anisotropic parameters of atomic displacements in $K_2Al_2B_2O_7$ at different

temperatures, Table S25: K–O (Å) bond lengths and O–K–O (°) angles in the $K_2Al_2B_2O_7$ structure at different temperatures, Table S26: B,Al–O (Å) bond lengths and O–B,Al–O (°) angles in the $K_2Al_2B_2O_7$ structure at different temperatures, Table S27: B/Al–O–B/Al (°) angles in the $K_2Al_2B_2O_7$ structure at different temperatures, Table S28: O–O–O (°) angles in the $K_2Al_2B_2O_7$ structure at different temperatures.

Acknowledgments: We are grateful to Yurij. F. Shepelev (1939–2009) for the single-crystal X-ray diffraction study of β-BaB_2O_4 at 693 K and α-BaB_2O_4 at 298 and 673 K. Yurij Shepelev was the first who refined borate crystal structures in the anharmonic approximation. We are thankful to Natalia Sennova for long-term productive cooperation in lithium borates area. We are thankful to Ludmila Isaenko for providing us with the single crystals of β-, α-BaB_2O_4 and $K_2Al_2B_2O_7$ used in this study. The study was supported by the Russian Foundation for Basic Research (project No. 15-03-05845). Powder HTXRD measurements of β- and α-BaB_2O_4 were performed at the Research Centre for X-ray Diffraction Studies of St. Petersburg State University.

Author Contributions: Rimma Bubnova, Stanislav Filatov, and Barbara Albert wrote the paper. Barbara Albert and Sergey Volkov performed the experiments and analysed the data.

Conflicts of Interest: The authors declare no conflict of interest.

References

1. Bloembergen, N. *Nonlinear Optics*; Benjamin: New York, NY, USA, 1965.
2. Schawlow, A.; Siegman, T. *Handbook of Nonlinear Optical Crystals*, 3rd ed.; Springer: Berlin, Germany, 1999.
3. Nikogosyan, D.N. *Nonlinear Optical Crystals: A Complete Survey*; Springer: New York, NY, USA, 1999.
4. Dalton, L.R.; Sullivan, P.A.; Bale, D.H. Electric Field Poled Organic Electro-optic Materials: State of the Art and Future Prospects. *Chem. Rev.* **2010**, *110*, 25–55.
5. Liu, X.; Yang, Z.; Wang, D.; Cao, H. Molecular Structures and Second-Order Nonlinear Optical Properties of Ionic Organic Crystal Materials. *Crystals* **2016**, *6*, 158.
6. Baldwin, G. *Nonlinear Optics*; Plenum: New York, NY, USA, 1969.
7. Zernicke, F.; Midwinter, J. *Applied Nonlinear Optics*; Wiley: New York, NY, USA, 1973.
8. Shen, Y. *The Principles of Nonlinear Optics*; Wiley: New York, NY, USA, 1984.
9. Yariv, A.; Yeh, P. *Optical Waves in Crystals*; Wiley: New York, NY, USA, 1984.
10. Kurtz, S.K.; Perry, J.T. A powder technique for the evaluation of nonlinear optical materials. *J. Appl. Phys.* **1968**, *39*, 3798–3813.
11. Chen, C.T.; Wu, Y.C.; Li, R.K. The relationship between the structural type of anionic group and SHG effect in boron-oxygen compounds. *Chin. Phys.* **1985**, *2*, 389–392.
12. Chen, C.; Sasaki, T.; Li, R.; Wu, Y.; Lin, Z.; Mori, Y.; Hu, Z.; Wang, J.; Uda, S.; Yoshimura, M.; et al. *Nonlinear Optical Borate Crystals*; Willey-VCH Verlag GmbH & Co. KGaA: Weinhaim, Germany, 2012.
13. Kidyarov, B.I.; Atuchin, V.V. Interrelationship of micro- and macro-structure with physical properties of binary acentric ferroelastic and paraelastic oxide crystal. *Ferroelectrics* **2007**, *360*, 104–107.
14. Dewey, C.F.; Cook, W.R.; Hodgson, R.T.; Wynne, J.J. Frequency doubling in KB_5O_8–$4H_2O$ and $NH_4B_5O_8$–$4H_2O$ to 217.3 nm. *Appl. Phys. Lett.* **1975**, *26*, 714–716.
15. Becker, P. Borate materials in nonlinear optics. *Adv. Mater.* **1998**, *10*, 979–992.
16. Chen, C.T.; Wu, B.C.; Jiang, A.D.; You, G.M. A new ultraviolet SHG crystal β-BaB_2O_4. *Sci. Sin.* **1985**, *18*, 235–243.
17. Chen, C.T.; Wu, Y.C.; Jiang, A.D.; Wu, B.C.; You, G.M.; Li, R.K.; Lin, S.J. New nonlinear-optical crystal LiB_3O_5. *J. Opt. Soc. Am.* **1989**, *6*, 616–621.
18. Wu, Y.C.; Sasaki, T.; Nakai, S.; Yokotani, A.; Tang, H.; Chen, C. CsB_3O_5: A new nonlinear optical crystal. *Appl. Phys. Lett.* **1993**, *62*, 2614–2615.
19. Chen, C.; Wang, Y.; Wu, B.; Wu, K. Design and synthesis of an ultraviolet-transparent nonlinear optical crystal $Sr_2Be_2B_2O_7$. *Nature* **1995**, *373*, 322.
20. Mori, Y.; Kuroda, I.; Nakajima, S.; Sasaki, T.;Nakai, S. Nonlinear optical properties of cesium lithium borate. *Jpn. J. Appl. Phys.* **1995**, 34, L296–L298.
21. Hu, Z.G.; Higashiyama, T.; Yoshimura, M.; Yap, Y.K.; Mori, Y.; Sasaki, T. A new nonlinear optical borate crystal $K_2Al_2B_2O_7$ (KAB). *Jpn. J. Appl. Phys.* **1998**, 37, L1093–L1094.
22. Ye, N.; Zeng, W.R.; Jiang, J.; Wu, B.C.; Chen, C.T.; Feng, B.H.; Zhang, X.L. New nonlinear optical crystal $K_2Al_2B_2O_7$. *J. Opt. Soc. Am.* **2000**, *17*, 764–768.
23. Hellwig, H.; Liebertz, J.; Bohaty, L. Exceptional large nonlinear optical coefficients in the monoclinic bismuth borate BiB_3O_6 (BIBO). *Solid State Commun.* **1999**, *109*, 249–251.

24. Barbier, J.; Penin, N.; Denoyer, A.; Cranswick, L.M. $BaBiBO_4$, a novel non-centrosymmetric borate oxide. *Solid State Sci.* **2005**, *7*, 1055–1061.
25. *Inorganic Crystal Structure Database (ICSD)*; National Institute of Standards and Technology: Gaithersburg, MD, USA, 2016.
26. Bubnova, R.S.; Filatov, S.K. High-temperature borate crystal chemistry. *Z. Kristallogr.* **2013**, *228*, 395–428.
27. Wright, A.C. Borate structures: Crystalline and vitreous. *Phys. Chem. Glass Eur. J. Glass Sci. Technol. B* **2010**, *51*, 1–39.
28. Burns, P.S.; Grice, J.D.; Hawthorne, F.C. Borate minerals. I. Polyhedral clasters and fundamental building blocks. *Can. Miner.* **1995**, *33*, 1131–1151.
29. Touboul, M.; Penin, N.; Nowogrocki, G. Borates: A survey of main trends concerning crystal-chemistry, polymorphism and dehydration process of alkaline and pseudo-alkaline borates. *Solid State Sci.* **2003**, *5*, 1327–1342.
30. Yuan, G.; Xue, D. Crystal chemistry of borates: The classification and algebraic description by topological type of fundamental building blocks. *Acta Cryst.* **2007**, B63, 353–362.
31. Hawthorne, F.C.; Burns, P.C.; Grice, J.D. The crystal chemistry of boron. *Rev. Miner.* **1996**, *33*, 41–116.
32. Strunz, H. Classification of borate minerals. *Eur. J. Miner.* **1997**, *9*, 225–232.
33. Grice, J.D.; Burns, P.C.; Hawthorne, F.C. Borate minerals. II. A hierarchy of structures based upon the borate fundamental building block. *Can. Miner.* **1999**, *37*, 731–762.
34. Filatov, S.K.; Bubnova, R.S. Borate Crystal Chemistry. *Phys. Chem. Glass* **2000**, *41*, 216–224.
35. Becker, P.A. A contribution to borate crystal chemistry: Rules for the occurrence of polyborate anion types. *Z. Kristallogr.* **2001**, *216*, 523–533.
36. Parthé, E. Calculation of the BO_3 triangle to BO_4 tetrahedron ratio in borates. *Z. Kristallogr.* **2002**, *217*, 179–200.
37. Parthé, E. New examples of crystallized and amorphous borates where the ratio of BO3 triangles to BO_4 tetrahedra can be calculated from the chemical formula. *J. Alloys Compd.* **2004**, *367*, 126–131.
38. Belokoneva, E.L. Borate crystal chemistry in terms of the extended OD theory: Topology and symmetry analysis. *Cryst. Rev.* **2005**, *11*, 151–198.
39. Belokoneva, E.L. Systematic, properties, and structure predictions of new borate materials. *Cryst. Res. Technol.* **2008**, *43*, 1173–1182.
40. Yu, D.; Xue, D. Bond analyses of borates from the Inorganic Crystal Structure Database. *Acta Cryst.* **2006**, B62, 702–709.
41. Hawthorne, F.C. The structure hierarchy hypothesis. *Min. Mag.* **2014**; 78, 957–1027.
42. Bubnova, R.S.; Filatov, S.K. Strong anisotropic thermal expansion in borates. *Phys. Stat. Solid.* **2008**, 245, 2469–2476.
43. Bubnova, R.; Filatov, S. *High-Temperature Crystal Chemistry Borates and Borosilicates*; Nauka: State Petersburg, Russian, 2008. (In Russian)
44. Filatov, S.K.; Bubnova, R.S. Atomic nature of the high anisotropy of borate thermal expansion. *Phys. Chem. Glasses Eur. J. Glass Sci. Technol.* **2015**, *56*, 24–35.
45. Bubnova, R.S.; Filatov, S.K. Self-assembly and high anisotropy thermal expansion of compounds consisting of TO_3 triangular radicals. *Struct. Chem.* **2016**, *27*, 1647–1662.
46. Bubnova, R.S.; Shepelev, J.F.; Sennova, N.A.; Filatov, S.K. Thermal behavior of the rigid-oxygen groups in the a-$Na_2B_8O_{13}$ crystal structure. *Z. Crystallogr.* **2002**, *217*, 444–450.
47. Shepelev, Y.F.; Bubnova, R.S.; Filatov, S.K.; Sennova, N.A.; Pilneva, N.A. LiB_3O_5 crystal structure at 20, 227 and 377 °C. *JSSC* **2005**, *178*, 2987–2997.
48. Filatov, S.; Bubnova, R.; Shepelev, Y.; Anderson, J.; Smolin, Y. The crystal structure of high-temperature α-CsB_5O_8 modification at 20, 300, and 500 °C. *Cryst. Res. Technol.* **2005**, *40*, 65–72.
49. Lu, S.F.; Huang, Z.X.; Huang, J.L. Meta-barium borate, II-BaB_2O_4, at 163 and 293 K. *Acta Crystallogr. C* **2006**, 62, i73–i75.
50. Sennova, N.A.; Bubnova, R.S.; Shepelev, Y.F.; Filatov, S.K.; Yakovleva, O.I. $Li_2B_4O_7$ Crystal structure in anharmonic approximation at 20, 200, 400 and 500 °C. *J. Alloys Compd.* **2007**, *428*, 290–296.
51. Sennova, N.A.; Bubnova, R.S.; Cordier, G.; Albert, B.; Filatov, S.K.; Isaenko, L. Temperature dependent changes of the crystal structure of $Li_2B_4O_7$. Z. *Anorg. Alloys Chem.* **2008**, *634*, 2601–2607.
52. Adamiv, V.T.; Burak, Y.V.; Teslyuk, I.M. The crystal structure of $Li_2B_4O_7$ compound in the temperature range 10–290 K. *J. Alloys Compd.* **2009**, *475*, 869–873.

53. Senyshyn, A.; Schwarz, B.; Lorenz, T.; Adamiv, V.T.; Burak, Y.V.; Banys, J.; Grigalaitis, R.; Vasylechko, L.; Ehrenberg, H.; Fuess, H. Low-temperature crystal structure, specific heat, and dielectric properties of lithium tetraborate $Li_2B_4O_7$. *J. Appl. Phys.* **2010**, *108*, 093524.
54. Senyshyn, A.; Boysen, H.; Niewa, R.; Banys, J.; Kinka, M.; Burak, Y.; Adamiv, V.; Izumi, F.; Chumak, I.; Fuess, H. High-temperature properties of lithium tetraborate $Li_2B_4O_7$. *J. Phys. D Appl. Phys.* **2012**, *45*, 175305.
55. Sennova, N.A.; Cordier, G.; Albert, B.; Filatov, S.K.; Bubnova, R.S.; Isaenko, L.I.; Prosenc, M.H. Temperature- and moisture-dependency of $CsLiB_6O_{10}$. A new phase, β-$CsLiB_6O_{10}$. *Z. Kristallogr.-Cryst. Mater.* **2010**, *229*, 741–751.
56. Fofanova, M.; Bubnova, R.; Albert, B.; Filatov, S.; Cordier, G.; Egorysheva, A. Structural changes in metastable γ-$Na_2B_4O_7$ between-150 °C and 720 °C. *Z. Kristallogr.* **2013**, *228*, 520–525.
57. Stein, W.D.; Cousson, A.; Becker, P.; Bohatý, L.; Braden, M. Temperature-dependent X-ray and neutron diffraction study of BiB_3O_6. *Z. Kristallogr.* **2007**, *222*, 680–689.
58. Volkov, S.N.; Bubnova, R.S.; Zalisskii, V.G.; Egorysheva, A.V.; Volodin, V.D.; Filatov, S.K. Thermal behavior of borate $BaBiBO_4$. *Glass Phys. Chem.* **2015**, *41*, 622–629.
59. Dinnebier, R.E.; Hinrichsen, B.; Lennie, A.; Jansen, M. High-pressure crystal structure of the non-linear optical compound BiB_3O_6 from two-dimensional powder diffraction data. *Acta Cryst.* **2009**, *B65*, 1–10.
60. Mighell, A.D.; Perloff, A.; Block, S. The crystal structure of the high temperature form of barium borate, $BaO{\cdot}B_2O_3$. *Acta Cryst.* **1966**, *20*, 819–823.
61. Krogh-Moe, J. Structural interpretation of melting point depression in the sodium borate system. *Phys. Chem. Glasses* **1962**, *3*, 101–105.
62. Krogh-Moe, J. Interpretation of the infra-red spectra of boron oxide and alkali borate glasses. *Phys. Chem. Glasses* **1965**, *6*, 46–54.
63. Huppertz, H.; Eltz, B. Multianvil high-pressure synthesis of $Dy_4B_6O_{15}$: The first oxoborate with edge-sharing BO4 tetrahedra. *J. Am Chem. Soc.* **2002**, *124*, 9376–9377.
64. Huppertz, H. High-pressure preparation, crystal structure, and properties of $RE_4B_6O_{15}$ (RE = Dy, Ho) with an extension of the "Fundamental Building Block" descriptors. *Z. Naturforsch.* **2003**, 58b, 278–290.
65. Huppertz, H. New synthetic discoveries via high-pressure solid-state chemistry. *Chem. Commun.* **2011**, *47*, 131–140.
66. Hazen, R.M.; Prewitt, C.T. Effect of temperature and pressure on interatomic distances in oxygen-based minerals. *Am. Miner.* **1977**, *62*, 309–315.
67. Hazen, R.M.; Finger, L.W. *Comparative Crystal Chemistry: Temperature, Pressure, Composition and the Variation of Crystal Structure*, 1st ed.; Wiley: London, UK, 1982.
68. Christ, C.L.; Clark, J.R. A crystal-chemical classification of borate structures with emphasis on hydrated borates. *Phys. Chem. Miner.* **1977**, *2*, 59–87.
69. Bokii, G.; Kravchenko, V. Crystal-chemical classification of borates. *J. Struct. Chem.* **1966**, *7*, 860–877.
70. Wu, H.; Yu, H.; Pan, S.; Huang, Z.; Yang, Z.; Su, X.; Poeppelmeier, K.R. $Cs_2B_4SiO_9$: A Deep-Ultraviolet Nonlinear Optical Crystal. *Angew. Chem. Int. Ed.* **2013**, *52*, 3406–3410.
71. Vitzthum, D.; Wurst, K.; Prock, J.; Brüggeller, P.; Huppertz, H. The New Indium Borate $In_{19}B_{34}O_{74}(OH)_{11}$ with T2 Supertetrahedra. *Inorg. Chem.* **2016**, *55*, 11473–11478.
72. Fröhlich, R.; Bohatý, L.; Liebertz, J. Die kristallstruktur von wismutborat, BiB_3O_6. *Acta Cryst.* **1984**, C40, 343–344.
73. Downs R.T.; Gibbs G.V.; Bartelmehs K.L.; Boisen M.B. Variations of bond lengths and volumes of silicate tetrahedra with temperature. *Am. Miner*. **1992**, *77*, 751–757.
74. Cruickshank, D.W.J. Errors in bond lengths due to rotational oscillations of molecules. *Acta Cryst*. **1997**, *9*, 757–758.
75. Busing, W.R.; Levy, H.A. The effect of thermal motion on the estimation of bond lengths from diffraction measurements. *Acta Cryst*. **1964**, *17*, 142–146.
76. Downs, R.T. Analysis of harmonic displacement factors. *Rev. Miner*. **2000**, *41*, 61–87.
77. Hazen R.M.; Downs R.T.; Prewitt C.T. Principles of comparative crystal chemistry. *Rev. Miner*. **2000**, *41*, 1–33.
78. Sennova, N.; Albert, B.; Bubnova, R.; Krzhizhanovskaya, M.; Filatov, S. Anhydrous lithium borate, $Li_3B_{11}O_{18}$, crystal structure, phase transition and thermal expansion. *Z. Kristallogr*. **2014**, *229*, 497–504.

79. Mathews, M.D.; Tyagi, A.K; Moorthy, P.N. High-temperature behaviour of lithium borates: Part II: High-temperature X-ray diffractometric and dilatometric studies. *Thermochim. Acta* **1998**, *319*, 113–121.
80. Wei, L.; Guiqing, D.; Qingzhen, H.; An, Z.; Jingkui, L. Anisotropic thermal expansion of LiB_3O_5. *J. Phys. D Appl. Phys*. **1990**, *23*, 1073.
81. Krzhizhanovskaya, M.G.; Sennova, N.A.; Bubnova R.S.; Filatov S.K. Thermal transformations of minerals: Borax–tincalconite–kernite. *Proc. Russ. Miner. Soc*. **1999**, *128*, 115–122.
82. Volkov, S.N.; Filatov, S.K.; Bubnova, R.S.; Ugolkov, V.L.; Svetlyakova, T.N.; Kokh, A.E. Thermal expansion and order-disorder polymorphic transformation in the family of borates $BaNaMe(BO_3)_2$, Me = Sc, Y. *Glass Phys. Chem.* **2012**, *38*, 162–171.
83. Sennova, N.A.; Bubnova, R.S.; Filatov, S.K.; Polyakova, I.G. High-temperature crystal chemistry of α-$Na_2B_4O_7$ and β-NaB_3O_5 layered borates. *Glass Phys Chem*. **2007**. 33, 217–225.
84. Bubnova, R.; Albert, B.; Georgievskaya, M.; Krzhizhanovskaya, M.; Hofmann, K.; Filatov, S. X-ray powder diffraction studies and thermal behaviour of $NaK_2B_9O_{15}$, $Na(Na_{.17}K_{.83})_2B_9O_{15}$, and $(Na_{.80}K_{.20})K_2B_9O_{15}$. *J. Solid State Chem.* **2006**, *179*, 2954–2963.
85. Zhang, C.; Wang, J.; Cheng, X.; Hu, X.; Jiang, H.; Liu, Y.; Chen, C. Growth and properties of $K_2Al_2B_2O_7$ crystal. *Opt. Mater*. **2003**, *23*, 357–362.
86. Bubnova, R.S.; Polyakova, I.G.; Anderson, Y.E.; Filatov, S.K. Polymorphism and thermal expansion of the MB_5O_8 crystalline modifications. *Phys. Chem. Glasses* **1999**, *25*, 183–194.
87. Bubnova, R.S.; Fundamenskii, V.S.; Filatov, S.K.; Polyakova, I.G. Crystal Structure and Thermal Behavior of KB_3O_5. *Dokl. Phys. Chem*. **2004**, *398*, 249–253.
88. Anderson, Y.E.; Filatov, S.K.; Polyakova, I.G.; Bubnova, R.S. Thermal Behavior of $M^+B_5O_6(OH)_4{\cdot}2H_2O$ (M^+= K, Rb, Cs) and Polymorphic Transformations of CsB_5O_8. *Phys. Chem. Glasses* **2004**, *30*, 450–460.
89. Krzhizhanovskaya, M.G.; Bubnova, R.S.; Bannova, I.I.; Filatov, S.K. Crystal structure of $Rb_2Ba_4O_7$. *Crystallogr. Rep*. **1997**, *42*, 226–231.
90. Krzhizhanovskaya, M.G.; Bannova, I.I.; Filatov, S.K.; Bubnova, R.S. Crystal structure and thermal expansion of $Rb_5B_{19}O_{31}$. *Crystallogr. Rep*. **1999**, *44*, 187–192.
91. Bubnova, R.S.; Krivovichev, S.V.; Shakhverdova, I.P.; Filatov, S.K.; Burns, P.C.; Krzhizhanovskaya, M.G.; Polyakova, I.G. Synthesis, crystal structure and thermal behavior of $Rb_3B_7O_{12}$, a new compound. *Solid State Sci.* **2002**, *4*, 985–992.
92. Krjijanovskaya, M.G.; Bubnova, R.S.; Filatov, S.K.; Belger, A.; Paufler, P.; Crystal structure and thermal expansion of β-RbB_5O_8 from powder diffration data. *Z. Kristallogr.* **2000**, *215*, 740–743.
93. Bubnova, R.S.; Krzhizhanovskaya, M.G.; Polyakova, I.G.; Trofimov, V.B.; Filatov, S.K. Thermal deformations and phase transitions of RbB_3O_5. *Inorg. Mater*. **1998**, *34*, 1119–1124.
94. Krizhizhanoivskaya, M.G. (Saint-Petersburg State University, Saint-Petersburg, Russia); Bubnova, R.S. (Grebenshchikov Institute of Silicate Chemistry, Saint-Petersburg, Russia); Filatov, S.K. (Saint-Petersburg State University, Saint-Petersburg, Russia), Personal communication, 2010.
95. Bubnova, R.; Dinnebier, R.E.; Filatov, S.; Anderson, J. Crystal structure, thermal and compositional deformations of β-CsB_5O_8. *Cryst. Res. Technol*. **2007**, 42, 143–150.
96. Anderson, J.E.; Bubnova, R.S.; Filatov, S.K.; Ugolkov, V.L.; Britvin, S.N. Thermal investigation of ammonioborite $(NH_4)_3[B_{15}O_{20}(OH)_8]{\cdot}4H_2O$. *Phys. Chem. Glasses* **2009**, *35*, 191–198.
97. Bubnova, R.S.; Anderson, J.E.; Krzhizhanovskaya, M.G.; Filatov, S.K. Crystal structure and thermal expansion of ammonium pentaborate $NH_4B_5O_8$. *Phys. Chem. Glasses* **2010**, *36*, 369–375.
98. Anderson, Yu. E.; Bubnova, R.S.; Filatov, S.K.; Polyakova, I.G.; Krzhizhanovskaya M.G. Thermal behaviour of larderellite, $NH_4[B_5O_7(OH)_2]{\cdot}H_2O$. *Proc. Russian Mineral. Soc.* **2005**, *134*, 103–109. (In Russian)
99. Kondratieva, V.V.; Filatov, S.K. Teplovoe rasshirenie gidroboratsita $CaMg[B_3O_4(OH)_3]_2{\cdot}3H_2O$. *Izvestia AN SSSR. Neorgan. Mater.* **1986**, *22*, 273–276. (In Russian)
100. Filatov, S.K.; Kondratieva, V.V. Anomalnoe teplovoe rasshirenie kolemanita $Ca[B_3O_4(OH)_3]{\cdot}H_2O$. *Izvestia AN SSSR. Neorgan. Mater*. **1980**, *16*, 475–481. (In Russian)
101. Filatov, S.K.; Krzhizhanovskaya, M.G.; Bubnova, R.S.; Shablinskii, A.P.; Belousova, O.L.; Firsova, V.A. Thermal expansion and structural complexity of strontium borates. *Struct. Chem*. **2016**, *27*, 1663–1671.
102. Volkov, S.N.; Bubnova, R.S.; Dusek, M.; Krzhizhanovskaya, M.G.; Ugolkov, V.L.; Obozova, E.D. Polymorphic transition of $Sr_2B_2O_5$ pyroborate. In Proceedings of the VIII National Crystal Chemical Conference, Suzdal, Russia, 30 May–3 June 2016.

103. Han, S.; Wang, J.; Li, J.; Guo, Y.; Wang,Y.; Zhao, L.; Zhang, Y.; R. Boughton, I. Flux growth and thermal properties of $LiBaB_9O_{15}$ single crystal. *Mater. Res. Bull*. **2012**, *47*, 464–468.
104. Filatov, S.K.; Nikolaeva, N.V.; Bubnova, R.S.; Polyakova, I.G. Thermal expansion of β-BaB_2O_4 and BaB_4O_7 borates. *Glass Phys. Chem.* **2006**. *32*, 471–478.
105. Volkov, S.N.; Bubnova, R.S.; Filatov, S.K.; Krivovichev, S.V. Synthesis, crystal structure and thermal expansion of a novel borate, $Ba_3Bi_2(BO_3)_4$. *Z. Kristallogr.* **2013**, *228*, 436–443.
106. Krivovichev, S.V.; Bubnova, R.S.; Volkov, S.N.; Krzhizhanovskaya, M.G.; Egorysheva, A.V.; Filatov, S.K. Preparation, crystal structure and thermal expansion of a novel layered borate, $Ba_2Bi_3B_{25}O_{44}$. *J. Solid State Chem.* **2012**, *196*, 11–16.
107. Filatov, S.; Shepelev, Y.; Bubnova, R.; Sennova, N.; Egorysheva, A.V.; Kargin, Y.F. The study of $Bi_3B_5O_{12}$: synthesis, crystal structure and thermal expansion of oxoborate $Bi_3B_5O_{12}$. *J. Solid State Chem*. **2004**, *177*, 515–522.
108. Krzhizhanovskaya, M.G.; Bubnova, R.S.; Egorysheva, A.V.; Kozin, M.S.; Volodin, V.D.; Filatov, S.K. Synthesis, crystal structure and thermal behavior of a novel oxoborate $SrBi_2B_4O_{10}$. *J. Solid State Chem*. **2009**, *182*, 1260–1264.
109. Filatov, S. K.; Shepelev, Yu. F.; Aleksandrova, Yu. V.; Bubnova, R. S. Structure of bismuth oxoborate $Bi_4B_2O_9$ at 20, 200, and 450°C. *Russ. J. Inorg. Chem*. **2007**, *52*, 21–27.
110. Bubnova, R.S.; Shablinskii, A.P.; Volkov, S.N.; Filatov, S.K.; Krzhizhanovskaya, M.G.; Ugolkov, V.L. Crystal structures and thermal expansion of $Sr_{1-x}Ba_xBi_2B_2O_7$ solid solutions. *Phys. Chem. Glasses* **2016**, *42*, 337–348.
111. Bubnova, R.S.; Krivovichev, S.V.; Filatov, S.K.; Egorysheva, A.V.; Kargin, Y.F. Preparation, crystal structure and thermal expansion of a new bismuth barium borate, $BaBi_2B_4O_{10}$. *J. Solid State Chem*. **2007**, *180*, 2, 596–603.
112. Bubnova, R.S.; Alexandrova, J.V.; Krivovichev, S.V.; Filatov, S.K.; Egorysheva, A.V. Crystal growth, crystal structure of new polymorphic modification, β-$Bi_2B_8O_{15}$ and thermal expansion of α-$Bi_2B_8O_{15}$. *J. Solid State Chem.* **2010**, *183*, 458–464.
113. Becker, P.; Bohatý, L. Thermal expansion of bismuth triborate. *Cryst. Res. Technol*. **2001**, *36*, 1175–1180.
114. Biryukov, Ya.P. (Grebenshchikov Institute of Silicate Chemistry, Saint-Petersburg, Russia); Siidra, E.N. (Saint-Petersburg State University, Saint-Petersburg, Russia); Filatov, S.K. (Saint-Petersburg State University, Saint-Petersburg, Russia); Krzhizhanovskaya, M.G. (Saint-Petersburg State University, Saint-Petersburg, Russia); Bubnova, R.S. (Grebenshchikov Institute of Silicate Chemistry, Saint-Petersburg, Russia) Personal communication, 2016.
115. Siidra, E.N.; Bubnova, R.S.; Krzhizhanovskaya, M.G. Synthesis and anisotropy of thermal expansion of polymorphic aragonite modification of λ-$NdBO_3$. *Fiz. Khim. Stekla* **2012**, *38*, 881–884.
116. Biryukov, Y.P. (Grebenshchikov Institute of Silicate Chemistry, Saint-Petersburg, Russia); Filatov, S.K. (Saint-Petersburg State University, Saint-Petersburg, Russia); Krzhizhanovskaya, M.G. (Saint-Petersburg State University, Saint-Petersburg, Russia); Bubnova, R.S. (Grebenshchikov Institute of Silicate Chemistry, Saint-Petersburg, Russia) Personal communication, 2016.
117. Biryukov, Y.P.; Bubnova, R.S.; Filatov, S.K.; Goncharov, A.G. Synthesis and thermal behavior of $Fe_3O_2(BO_4)$ oxoborate. *Glass Phys. Chem*. **2016**, *42*, 202–206.
118. Lou, Y.; Li, D.; Li, Z.; Jin, S.; Chen, X. Unidirectional thermal expansion in edge-sharing BO_4 tetrahedra contained $KZnB_3O_6$. *Sci. Rep*. **2015**, 5, 10996.
119. Jiang, X.; Molokeev, M.S.; Gong, P.; Yang, Y.; Wang, W.; Wang, S.; Wu, S.; Wang, Y.; Huang, R.; Li, L.; et al. Near-Zero Thermal Expansion and High Ultraviolet Transparency in a Borate Crystal of $Zn_4B_6O_{13}$. *Adv. Mater.* **2016**. 28, 7936–7940.
120. Yao, W.; Jiang, X.; Huang, R.; Li, W.; Huang, C.; Lin. Z.; Li, L; Chen, C. Area negative thermal expansion in a beryllium borate $LiBeBO_3$ with edge sharing tetrahedra. *Chem. Commun*. **2014**, *50*, 13499–501.
121. Segonds, P.; Boulanger, B.; Ménaert, B.; Zaccaro, J.; Salvestrini, J.P.; Fontana, M.D.; Moncorgé, R.; Porée, F.; Gadret, G.; Mangin, J.; et al. Optical characterizations of YCa4O(BO3)3 and Nd:YCa4O(BO3)3 crystals. *Opt. Mater.* **2007**, *29*, 975–982.
122. Jing, F.; Fu, P.; Wu. Y.; Zu. Y.; Wang. X.; Growth and assessment of physical properties of a new nonlinear optical crystal: lanthanum calcium borate. *Opt. Mater*. **2008**, *30*, 1867–1872.
123. Zhang, J.; Zhang, G.; Li, Y.; Wu, Y.; Fu, P.; Wu, Y. Thermophysical Properties of a New Nonlinear Optical $Na_3La_9O_3(BO_3)_8$ Crystal. *Cryst. Growth Des*. **2010**, *10*, 4965–4967.

124. Radaev, S.F.; Maximov, B.A.; Simonov, V.I.; Andreev, B.V.; D'yakov, V.A. Deformation density in lithium triborate, LiB_3O_5. *Acta Cryst*. **1992**, B48, 154–160.
125. Xue, D.; Betzler, K.; Hesse, H. Chemical-bond analysis of the nonlinear optical properties of the borate crystals LiB_3O_5, $CsLiB_6O_{10}$, and CsB_3O_5. *Appl. Phys. A*. **2002**, *74*, 779–782.
126. Chen, Q.; Luo, M. Synthesis, Crystal Structure, and Nonlinear Optical Properties of a New Alkali and Alkaline Earth Metal Carbonate $RbNa_5Ca_5(CO_3)_8$. *Crystals* **2017**, *7*, 10.
127. Fröhlich, R. Crystal structure of the low-temperature form of BaB_2O_4. *Z. Kristallogr*. **1984**, *168*, 109–112.
128. Fedorov, P.P.; Koh, A.E.; Kononova, N.G. Barium borate β-BaB_2O_4 as material for nonlinear optics. *Russ. Chem. Rew*. **2002**, *71*, 741–763.
129. König, H.; Hoppe, R. Über borate der alkalimetalle. II. Zur Kenntnis von LiB_3O_5. *Z. Annorg. Allg. Chem*. **1978**, 439, 71–79.
130. Ihara, M.; Yuge, M.; Krogh-Moe, J. Crystal structure of lithium triborate $Li_2O{\cdot}3B_2O_3$. *J. Ceram. Soc. Jpn*. **1980**, *88*, 179.
131. Hénaff, C.; Hansen, N.K.; Protas, J.; Marnier, G. Electron Density Distribution in LiB_3O_5 at 293 K. *Acta Crystallogr*. **1997**, B53, 870–879.
132. Kaduk, J.A.; Satek, L.C.; McKenna, S.T. Crystal structures of metal aluminium borates. *Rigaku J*. **1999**, 16, 17–30.
133. Wang, Y.; Wang, L.; Gao, X.; Wang, G.; Li, R.K.; Chen, C.T. Growth, characterization and the fourth harmonic generation at 266 nm of $K_2Al_2B_2O_7$ crystals without UV absorptions and Na impurity. *J. Cryst. Growth*. **2012**, *348*, 1–4.
134. Hu, Z.-G.; Higashiyama, T.; Yoshimura, M.; Mori, Y.; Sasaki, T.; Redetermination of the crystal structure of dipotassium dialuminum borate, $K_2Al_2B_2O_7$, a new non-linear optical material. *Z. Kristallogr*. **1999**, *214*, 433–434.
135. Isaenko, L.I.; Dragomir, A.; McInerney, J.G.; Nikogosyan, D.N. Anisotropy of two-photon absorption in BBO at 264 nm. *Opt. Commun*. **2001**, *198*, 433–438.
136. Gets, V.A.; Il'ina O.S.; Isaenko L.I. Specific features of the flux growth of bulk crystals of high-temperature modification of BaB_2O_4. *Cryst. Rep*. **2006**, *51*, 508–512.
137. Ogorodnikov, A.N.; Pustovarov, V.A.; Yakovlev, S.A.; Isaenko, L.I.; Zhurkov, S.A. A time-resolved luminescence spectroscopy study of non-linear optical crystals $K_2Al_2B_2O_7$. *J. Lumin*. **2012**, *132*, 1632–1638.
138. Sheldrick, G.M. A short history of SHELX SHELXL-97. *Acta Cryst*. **2008**, *A64*, 112–122.
139. Petricek, V.; Dusek, M.; Palatinus, L. Crystallographic computing system JANA2006: General features. *Z. Kristallogr*. **2014**, *229*, 345–352.
140. Willis, B.T.M.; Pryor, A.W. *Thermal Vibrations in Crystallography*; Cambridge University Press: London, UK, 1975.
141. Momma, K.; Izumi, F. VEST A: A three-dimensional visualization system for electronic and structural analysis. *J. Appl. Crystallogr*. **2008**, *41*, 653–658.
142. Bubnova, R.S.; Firsova V.A.; Filatov S.K. Software for determining the thermal expansion tensor and the graphic representation of its characteristic surface (theta to tensor-TTT). *Glass Phys. Chem*. **2013**, *39*, 347–350.